

# 1 **The Capability of Sentinel-MSI (2A/2B) and Landsat-OLI (8/9)** 2 **for Seagrass and Algae Species Differentiation using Spectral** 3 **Reflectance**

4 Abderrazak Bannari <sup>1</sup>, Thamer Salim Ali <sup>2</sup> and Asma Abahussain <sup>2</sup>

5 <sup>1</sup>Space Pix-Map International Inc., Gatineau (Québec) J8R 3R7, Canada

6 <sup>2</sup>Department of Natural Resources and Environment, College of Graduate Studies, Arabian Gulf University, Manama,  
7 Kingdom of Bahrain, P.O. Box: 26671, Tel: (973) 1723-9545; Fax: (973) 1723-9552.

8  
9 Correspondence to: Abderrazak Bannari, Email: [abannari@bell.net](mailto:abannari@bell.net)

10  
11 **Abstract.** This paper assesses the reflectance difference values between the respective spectral bands in the visible  
12 and near-infrared (VNIR) of Sentinel-MSI-2A/2B and Landsat-OLI-8/9 sensors for seagrass, algae, and mixed species  
13 discrimination and monitoring in a shallow marine environment southeastern of Bahrain Island in the Arabian Gulf.  
14 To achieve these, a field survey was conducted to collect samples of seawater, underwater sediments, seagrass  
15 (*Halodule uninervis* and *Halophila stipulacea*) and algae (green and brown). As well, an experimental mode was  
16 established in a Goniometric-Laboratory to simulate the marine environment, and spectral measurements were  
17 performed using an ASD spectroradiometer. Measured spectra and their transformation using continuum-removed  
18 reflectance spectral (CRRS) approach were analyzed to assess spectral separability among separate or mixed species  
19 at varying coverage rates. Afterward, the spectra were resampled and convolved in the solar-reflective spectral bands  
20 of MSI and OLI sensors and converted into water vegetation indices (WVI) to investigate the potential of red, green,  
21 and blue bands for seagrass and algae species discrimination. The results of spectral and CRRS analyses highlighted  
22 the importance of the blue, green, and NIR wavelengths for seagrass and algae detection and likely discrimination  
23 based on hyperspectral measurements. However, when resampled and convolved in MSI and OLI bands, spectral  
24 information loses the specific and unique absorption features and becomes more generalized and less precise.  
25 Therefore, relying on the multispectral bandwidth of MSI and OLI sensors, it is difficult or even impossible to  
26 differentiate or to map seagrass and algae individually at the species level. Instead of the red band, the integration of  
27 the blue or the green bands in WVI increases their power to discriminate submerged aquatic vegetation (SAV),  
28 particularly WAVI, WEVI, and WTDVI indices. These results corroborate the spectral and the CRRS analyses.  
29 However, despite the power of blue wavelength to penetrate deeper into the water, it also leads to a relative  
30 overestimation of dense SAV coverage due to more scattering in this part of the spectrum. Furthermore, statistical fits  
31 ( $p < 0.05$ ) between the reflectance in the respective VNIR bands of SMI and OLI revealed excellent linear relationships  
32 ( $R^2$  of 0.999) with insignificant RMSD ( $\leq 0.0015$ ). Important agreements ( $0.63 \leq R^2 \leq 0.96$ ) were also obtained  
33 between respective WVI regardless of the integrated spectral bands (i.e., red, green, and blue), yielding insignificant  
34 RMSD ( $\leq 0.01$ ). Accordingly, these results pointed out that MSI and OLI sensors are spectrally similar, and their data  
35 can be used jointly to monitor accurately the spatial distribution of SAV and its dynamic in time and space in shallow  
36 marine environment, provided that rigorous data pre-processing issues are addressed.

## 37 1. Introduction

38 Seagrass meadows are identified as an important key for the characterization of environmental resources in estuarine  
39 and shallow coastal areas, and a fundamental health index allowing the assessment of coastal ecosystems. The  
40 composition and density of their species depend largely on water depth, temperature, salinity, coastal substrate  
41 material, and light penetration (Dierssen et al., 2015). Adapted to grow in shallow seawater down to a depth of 20 m,  
42 where approximately only 11% of surface light reaches the bottom (Duarte and Gattuso, 2008), they play an essential  
43 role in the sustainability of global ecosystem biodiversity in most shallow near-shore areas around the world (Den-  
44 Hartog, 1970; Konstantinos *et al.*, 2016). Moreover, the biodiversity of seagrass provides secure habitat and food for  
45 a wide variety of marine micro-organisms, improve the quality of water and protect shorelines against erosion in the  
46 middle and lower intertidal and sub-tidal zones (Roelfsema *et al.*, 2009; Anders and Lina, 2011; Yang and Yang,  
47 2012; Morrison *et al.*, 2014). Like other vegetation cover, seagrass beds play an important role in carbon storage  
48 (Novak and Short, 2020), as well as effective removal of carbon dioxide from the “biosphere-atmosphere” system,  
49 which significantly mitigates the climate change impacts (Duarte et al., 2013; Lyimo, 2016). Although occupying only  
50 0.2% of the world’s oceans (Traganos, 2020), seagrass beds can store twice as much per unit area as forests, and  
51 sequester around 10% of the total carbon received by the oceans (Fourqurean et al., 2012).

52 Unfortunately, natural and anthropogenic disturbances and disasters have led to the decline of seagrass around the  
53 world (Green and Short, 2003; Orth et al., 2006; Grech et al., 2012; Wood, 2012) at local and regional scales.  
54 Undoubtedly, these causes substantially destroy the seagrass beds and biota associated in such habitat and unbalance  
55 the ecological functions of coastal zones. Short et al. (2011) showed that seagrass habitat disappeared worldwide at a  
56 rate of 110 km<sup>2</sup> per year between 1980 and 2006. Hence, understanding the spatial distribution of seagrass biomass,  
57 its extent, condition, and change over time is essential for their monitoring, management, and protection (Short and  
58 Coles, 2001; Waycott *et al.*, 2009). Such monitoring provides updated and accurate information useful for the  
59 protection of several ecosystems (Leleu et al., 2012), conservation (Hamel and Andréfouët, 2010), coastal risk  
60 assessment (Warren et al., 2016), ecological resources development (Boström et al., 2011), and marine spatial  
61 planning (Saarman et al., 2012; Kibele, 2017). In addition, mapping and inventorying the total aboveground biomass  
62 of seagrass and algae are important for ecosystem health assessment (Short and Wyllie-Echeverria, 1996), alteration  
63 and dynamics in space-time (Neckles et al., 2012), biomass productivity and its contribution to the global biosphere  
64 carbon sink capacity (Waycott et al., 2009), and understanding the impacts of climate change (Hashim et al., 2014).

65 In the Arabian Gulf, the extreme environmental conditions combined with major seasonal variations in the marine  
66 environment promote the development of three seagrass species including *Halodule uninervis* which is the most  
67 dominant species, *Halophila stipulacea* that is less common, and *Halophila ovalis*, which is widely scattered and  
68 rarely forms relatively dense meadows. Along the western coast of the Arabian Gulf, these three species are reported  
69 and several species of marine algae are described, especially green and brown algae (Erfteimeijer and Shuail, 2012).  
70 This natural resource is located in shallow waters with depths ranging from the intertidal zone to 20 m, supporting the  
71 second largest population of dugongs (*Dugong dugon*) in the world (Preen, 2004); as well as a large population of  
72 Green Turtles (*Chelonia mydas*) and Hawksbill Turtles (*Eretmochelys imbricata*) (Thakur et al., 2007). Unfortunately,  
73 these coastal ecosystems are under continuous threats from anthropogenic activities (Waycott et al., 2009), such as

74 reclamation and dredging where several coastal developmental projects are constructed and others under construction  
75 (small islands projects development), industrial effluents, oil exploration, pipeline laying, maritime transportation,  
76 intensive circulation of commercial fishing boats, pollution and discharges of seawater desalinization and wastewater  
77 into the sea (Onuf, 1994; Dunton and Schonberg, 2002; Burfeind and Stunz, 2006; Naser, 2011; Erfteimeijer and  
78 Shuail, 2012). Eventually, these activities catalyze the degradation and destruction of seagrass species and related  
79 ecosystems. Therefore, the assessment of seagrass conditions associated with broad scale of benthic species should be  
80 based on relevant and accurate information to measure several health indicators of coastal areas to ensure the  
81 sustainable development of these natural resources.

82 Previously, photo-interpretation approaches based on aerial photography have been adopted to follow seagrass and  
83 algae species development and assessment in space and time (Ferguson and Wood, 1990; Meehan et al., 2005; Mount,  
84 2007). Afterward, the first generation of satellite remote sensing was used to investigate the seagrass classes'  
85 composition, differentiation, classification, etc. (Hossain et al., 2014; Komatsu et al., 2020). Unfortunately, these goals  
86 were difficult to achieve accurately because the radiometric and spectral resolutions of sensors lacked the sensitivity  
87 to discriminate among different marine vegetation species and fragmented classes (Mumby et al., 1997; Wicaksono  
88 and Hafizt, 2013). To improve land-water surfaces reflectivity and information extraction, recent developments in  
89 remote sensing science and technology have led to an improvement of sensors performance in spatial and spectral  
90 resolutions, assuming a potential mapping of the marine environment and aquatic vegetation at the species level;  
91 obviously, if species under investigation have distinct spectral signatures. For instance, the Multi-Spectral Instruments  
92 (MSI) onboard Sentinel 2A and 2B, as well as the Operational Land Imager (OLI) sensors onboard Landsat 8 and 9  
93 platforms were designed with a significant improvement of the signal-to-noise ratio (SNR) and radiometric  
94 performances (Knight and Kvaran, 2014). The availability of this new generation of sensors offers innovative  
95 opportunities for long-term high-temporal frequency for Earth surfaces' observation and monitoring (Mandanici and  
96 Bitelli, 2016). The free availability of their data significantly advances the applications of remote sensing with medium  
97 spatial resolutions (Roy et al., 2014; Wulder et al., 2015; Zhang et al., 2018). Thanks to the improvement of their  
98 spectral, radiometric, and temporal resolutions, they can expand the range of their applications to several natural  
99 resources and environmental domains for monitoring, assessing, and investigating (Hedley et al., 2012a and 2012b).  
100 Moreover, the orbits of these four satellites constellation (Sentinel 2A and 2B and Landsat 8 and 9) are designed to  
101 ensure a revisiting interval time of less than 2 days (Li and Roy, 2017; Li and Chen, 2020), thereby substantially  
102 increasing the monitoring capabilities of the Earth's surface and ecosystems (Drusch et al., 2012). Their spectral  
103 resolutions and configurations are designed in such a way that there is a significant match between the homologous  
104 spectral bands, i.e. closely related spectral filters position and bandwidths (Drusch et al., 2012; Irons et al., 2012).  
105 However, depending on the sensitivity of the intended application (Flood, 2017), the sensor radiometric drift  
106 calibration (Markham et al., 2016), the atmospheric corrections (Vermote et al., 2016), the surface reflectance  
107 anisotropy (Roy et al., 2017), and the sensors co-registration (Skakun et al., 2017; Yan et al., 2018), it is plausible that  
108 the natural surface-reflectances recorded by MSI and OLI sensors over the same target in the marine environment may  
109 be different. In addition, the relative spectral response profiles characterizing the filters (spectral responsivities) of  
110 these instruments are not perfectly identical between the homologous bands, so some differences are probably

111 expected over the recorded land or water surfaces reflectance values and, therefore, their data cannot be reliably used  
112 together (Bannari et al., 2004; Van-derWerff and Van-der-Meer, 2016; Bannari, 2019). The importance of these  
113 differences depends on the application (spectral characteristics of the observed target) and on the approach adopted to  
114 perform time-series analyses, mapping, or change detection exploiting these instruments (Flood, 2017). For instance,  
115 it is plausible that the extraction of seagrass and/or algae information in time over shallow water areas using surface  
116 reflectances, empirical, semi-empirical, and/or physical approaches, may affect the comparison of the results.

117 The main objectives of this research focus on the analysis of Sentinel-MSI and Landsat-OLI homologous visible  
118 and near-infrared (VNIR) bands capability to distinguish and discriminate among seagrass (*Halodule uninervis* and  
119 *Halophila stipulacea*), algae (green and brown), and any probable case of mixed species of seagrass and algae sampled  
120 from the southeast area of Bahrain national water. To achieve these, the specific following steps are considered. 1)  
121 Examination of spectral signatures in VNIR wavelengths and their continuum-removal transformations for potential  
122 differentiation among the considered seagrass and algae species and their mixture submerged in seawater at different  
123 coverage rates, as well as considering the sediment-substrate with bright and dark colors. 2) Comparison and analysis  
124 of the difference between the resampled and convolved reflectances in the VNIR homologous bands of MSI and OLI  
125 sensors considering all examined samples. 3) Comparison between MSI and OLI sensors in terms of converting the  
126 reflectances over the considered samples at different coverage rates into several water vegetation indices (WVI).  
127 Finally, 4) efficiency and accuracy analysis of the examined WVI to discriminate between species (seagrass, algae  
128 and mixed) by integrating the green and blue bands instead of the red band. Further, according to these analyses  
129 results, it will be clear whether it is possible for these sensors to differentiate between seagrass and algae effectively  
130 and precisely at the species level, or simply and generally to discriminate among submerged aquatic vegetation (SAV)  
131 cover at different density classes. Moreover, to place this research in the international context, the following section  
132 reviews the use of remote sensing (sensors and methods) for the detection, discrimination and mapping of different  
133 seagrass and algal species in many coastal locations around the world.

## 134 **2. Remote sensing of seagrass and algae detection and mapping: A review**

135 Traditional seagrass *in-situ* surveys require time and intensive field sampling, which generally lack the spatial  
136 coverage and precision that are required to detect changes before they become irreversible or are very difficult to  
137 maintain year after year (Peterson and Fourqurean, 2001; Yang and Yang, 2012). Over the recent decades, remote  
138 sensing science and sensors technology has played an essential role in seagrass mapping and monitoring (Dean and  
139 Salim, 2013; Dierssen et al., 2015). According to literature, the mapping of the characteristics and properties of  
140 seagrass and algae in the marine environment occurs over relatively small areas with limited variations in water depth  
141 and clarity using satellite, airborne, and drone remote sensing sensors (multispectral and hyperspectral). Moreover,  
142 field and laboratory *in-situ* measurements have been conducted for calibration and validation in several environments  
143 around the world (Larkum et al., 2006; Roelfsema et al., 2009; Hossain et al., 2014; Komatsu et al., 2020; Duffy et  
144 al. 2018).

145 Under laboratory conditions using spectral measurements, Thorhaug et al. (2007) demonstrated the near similarity  
146 in the shape and form of the spectral signatures of three different seagrass species with a very slight difference and

147 pointed out subtle differences between marine algae (green and brown) and seagrass. In the central west coast of  
148 Florida in the USA, Pu *et al.* (2012) used *in-situ* Hyperspectral measurements in the field and laboratory to analyse  
149 the spectral behaviour and the potential discrimination among several seagrass species according to their spatial extent  
150 and abundance, water depths, and substrate types. They highlighted that the discrimination of seagrass species and the  
151 percentage of SAV coverage are affected by water depth and substrate on the measured spectra. Moreover, Wood  
152 (2012) demonstrated the potential of the synergy between the field spectra and hyperspectral data for seagrass sensing  
153 and mapping in Redfish Bay, Texas in the USA. Exploiting modeled and simulated data, Hedley *et al.* (2012a)  
154 demonstrated that Sentinel-MSI has an improved capability for detection and discrimination of the marine  
155 environment compared to SPOT-4 and Landsat-ETM+. Furthermore, Fyfe (2003) reported that the spectral signatures  
156 measured on harvested wet leaves (out of water) of different seagrass species were spectrally distinct. However, the  
157 real marine environment conditions are different from wet leaves due to water-column constituents including  
158 phytoplankton, suspended organic and inorganic matter, water depth variability, and optical properties of the  
159 underlying sediments (Pu *et al.*, 2012).

160 Otherwise, NASA's Landsat program is the earliest and most commonly used over the past five decades. It consists  
161 of a series of nine satellite missions using four types of multispectral sensors including MSS, TM, ETM +, and OLI  
162 (Bannari and Al-Ali, 2020). These sensors have been used by many scientists to detect and map seagrass beds at local  
163 and regional scales (Phinn *et al.* 2008; Knudby and Nordlund, 2011; Lyons *et al.* 2012 and 2013; Kovacs *et al.* 2018).  
164 Exploring a time-series of 23 annual images acquired over the Eastern Banks of Moreton Bay in Australia, Lyons *et al.*  
165 (2013) demonstrated how TM and ETM+ data time-series analysis enabled seagrass spatial distribution to be  
166 appropriately assessed spatiotemporally. Moreover, a regional-scale mapping of seagrass habitat in the Wider-  
167 Caribbean region was achieved with acceptable accuracies using a total of 40 scenes acquired with TM and ETM+  
168 sensors, and applying different images processing methods (Wabnitz *et al.*, 2008). In Cam-Ranh Bay in Vietnam,  
169 Chen *et al.* (2016) investigated the temporal changes of seagrass beds over 20 years (1996 to 2015) by exploiting  
170 multi-temporal Landsat data acquired with TM, ETM+ and OLI sensors. Dekker *et al.* (2005) demonstrated that TM  
171 and ETM+ instruments did not have sufficient spectral and radiometric resolutions to discriminate among three  
172 seagrass species in a shallow coastal Australian lake. Contrariwise, Dahdouh-Guebas *et al.* (1999) reported the utility  
173 of TM data associated with ground truth measurements to map accurately the distribution of seagrass and algae on the  
174 Kenyan coast. In addition to the Landsat sensor series, the European satellites such as SPOT-HRV were also used in  
175 combination with *in-situ* spectroradiometric measurements and quantitative semi-empirical models to assess the  
176 changes in the spatial distribution of seagrass biomass in Bourgneuf-Bay in France over 14 years (Barillé *et al.* 2010).  
177 Likewise, the potential of the Indian satellite (IRS-ID LISS-III) has been demonstrated for mapping the seagrass  
178 meadows extent in the Gulf of Mannar Biosphere Reserve in India (Umamaheswari *et al.*, 2009).

179 Furthermore, the first generation of commercial satellites operated by the private remote sensing industry with  
180 very high spatial resolution and narrow spectral resolutions, such as IKONOS, Quickbird, WorldView, etc., offers  
181 complementary technology for seagrass sensing and mapping. This new technology provides an excellent compromise  
182 between spatial and spectral resolutions for information extraction. In clear water seagrass habitat in the Moreton-Bay  
183 (Australia), the spatial and temporal dynamics of seagrasses (cover, species, and biomass) have been studied from the

184 leaf to patch scales between 2004 and 2013 integrating nine high spatial resolutions images acquired with WorldView-  
185 2, IKONOS, and Quickbird-2 and applying object-image processing approach (Roelfsema *et al.*, 2014). The results  
186 showed the utility of this new spatial technology for time-series analysis and the derivation of seagrass products that  
187 are very useful in marine ecology management. Moreover, Knudby and Nordlund (2011) highlighted the utility of  
188 IKONOS data for multi-species of seagrass detection in a patchy environment around Chumbe Island in Zanzibar  
189 (Tanzania). Along Zakynthos Island in Greece, Pasqualini *et al.* (2005) demonstrated that the SPOT-5 data with 2.5  
190 and 10 m spatial resolutions are suitable for seagrass classes' classification according to the overall accuracies. In  
191 shallow waters of Moreton Bay in Australia, Phinn *et al.* (2008) have shown that the spatial and spectral resolutions  
192 of multispectral (Quickbird and Landsat-TM) and hyperspectral (airborne CASI) data affects the precision of seagrass  
193 biomass differentiation at the species level, i.e., when the pixel size increases the error is getting higher. Contrary to  
194 these findings, in the Capo Rizzuto area in Italy, Dattola *et al.* (2018) reported the potential of the high spatial  
195 resolution of WorldView-2 compared to the medium resolution of MSI and OLI for different seagrass species  
196 characterization. In addition, to identify the spatial distribution of seagrass beds in Xincun Bay (Hainan province in  
197 China), Yang and Yang (2009) demonstrated that Quickbird data are more accurate than those of TM and CBERS  
198 (China-Brazil Earth Resources Satellite data) sensors.

199 In addition to remote sensing sensor technologies, a variety of image processing methods have been employed in  
200 mapping seagrass spatial distribution and coverage. For instance, Marcello *et al.* (2018) demonstrated the good  
201 performance of support vector machines (SVM) approach compared to spectral angle mapper (SAM) and maximum  
202 likelihood for seagrass classification; moreover, they pointed out the greater aptitude of hyperspectral compared to  
203 multispectral data. Likewise, Peneva *et al.* (2008) reported that the maximum likelihood classification produced the  
204 highest overall accuracy while SAM yielded the lowest accuracy due to the predominant influence of water-column  
205 optical properties on the apparent spectral characteristics of seagrass and sand bottom in the northern Gulf of Mexico.  
206 For *Posidonia oceanica* mapping in the Mediterranean region, the random forests method gives more accurate results  
207 than SVM approaches when compared with in-situ observations (Bakirman and Gumusay, 2020). Whereas, using a  
208 high spatial resolution of WorldView-2 imagery acquired over a coastal area in Florida, the neural network classifier  
209 performed better than SVM for seagrass mapping (Perez *et al.*, 2020). According to Uhrin and Townsend (2016),  
210 linear spectral mixture analysis (LSMA) can be used with photo interpretation to generate spatially resolved maps  
211 suitable for seagrass spatial distribution and provide improved estimates of seagrass classes. Nevertheless, Chen *et al.*  
212 (2016) revealed the difficulty and limitation of LSMA for mapping the fraction of scattered and heterogeneous  
213 seagrass patches that are smaller than the pixel size. At Ritchie's archipelago within the Andaman and Nicobar group  
214 of Islands, Bayyana *et al.* (2020) showed that Sentinel-MSI data can detect, and map submerged benthic habitat and  
215 seagrass beds present at a depth of 21 m using random forest, SVM, and K-nearest-neighbour classification algorithms.  
216 Besides, linear regressions were established between the field truth measurements and several vegetation indices  
217 derived from SPOT-XS, Landsat-TM, and CASI Hyperspectral airborne, to measure the density of seagrass in the  
218 tropical Western Atlantic (Mumby *et al.*, 1997).

219 Since the emergence of remote sensing as a new scientific discipline in the early 1970s, vegetation indices (VI's)  
220 were involved as radiometric measurements of the spatial and temporal distribution of photo-synthetically active land

221 vegetation. They use the red and near-infrared (NIR) bands, the normalized difference vegetation index (NDVI) was  
222 proposed by Rouse et al. (1974) at the dawn of remote sensing. Since these two spectral bands are generally present  
223 on Earth observation and meteorological satellites, and often containing more than 90% of the information relating to  
224 vegetation canopy (Bannari et al., 1995), the NDVI had taken a privileged place in the NASA/NOAA Pathfinder  
225 project (James and Kalluri, 1994). Thus, it was daily derived from NOAA-AVHRR data at the Earth scale.  
226 Subsequently, it was also derived every day from MODIS and SPOT-Vegetation data to produce time-series products  
227 for global vegetation assessment and monitoring at the regional and global scales. Due to this glorious history and its  
228 simplicity, the NDVI has become the most widely used to assess vegetation canopy. Then, this index was improved  
229 in a new version named soil adjusted vegetation index (SAVI) by Huete (1988) to minimize the artefacts caused by  
230 soil background on the estimation of vegetation cover fraction by incorporating a correction factor “L”. To overcome  
231 the limitations of linearity and saturation, to reduce the noise of atmospheric effects, and to remove the artefacts of  
232 soil optical properties, the enhanced vegetation index (EVI) was proposed also by Huete *et al.* (2002). Likewise, the  
233 transformed difference vegetation index (TDVI) was developed by Bannari *et al.* (2002) to describe the vegetation  
234 cover fraction independently to the background artefacts, to reduce the saturation problem, and to enhance the  
235 vegetation dynamic range linearly. These indices (NDVI, SAVI, EVI, and TDVI) were used to establish a close  
236 relationship between radiometric responses and land vegetative cover densities, and they were implemented in the  
237 ENVI image processing system.

238 In marine applications, several scientists tested these indices for seagrass and algae discrimination and mapping.  
239 The NDVI extracted from SPOT-HRV images coupled with *in-situ* spectroradiometric data provided satisfactory  
240 results for spatiotemporal change of seagrass beds in Bourgneuf-Bay in France (Barillé et al., 2009). Using  
241 hyperspectral data, Dierssen et al. (2015) reported the potential of NDVI for SAV classes’ discrimination. Similarly,  
242 Zoffoli et al. (2020) demonstrated the capability of NDVI derived from Sentinel-MSI data for seagrass percent cover  
243 estimation and leaf biomass mapping to characterize its seasonal dynamics along the European Atlantic coast.  
244 However, although VNIR bands are generally available in optical remote sensing satellites, it is well known that only  
245 the visible bands can penetrate ocean water deeper than NIR which is largely absorbed by the water surface (Kirk,  
246 1994). Thus, regardless of the concentrations of suspended sediments and/or organic matter, the visible wavelengths  
247 are used to map the marine environment. Indeed, the blue penetrates deeper (~ 37 m) than any other wavelengths,  
248 followed by green (~ 30 m), then red (~ 7 m), and NIR (Fig. 1) penetrates the least, being attenuated in the shallowest  
249 depths around 2.5 m (Komatsu et al., 2020). Accordingly, blue, green, and red are the most suitable for sensing  
250 seagrass and SAV (Silva et al., 2008). Thereby, when vegetation indices are applied in the marine environment  
251 (Davranche et al., 2010; Zhao et al., 2013), always the red band is substituted by that of blue or green. Then, discussion  
252 was initiated on WVI or aquatic vegetation indices (AVI). For instance, when the red was replaced by the green in  
253 NDVI (Yang and Yang, 2009) and by the blue in SAVI (Villa et al., 2013) these versions were named, respectively,  
254 the Normalized Difference Aquatic Vegetation Index (NDAVI or WNDVI) and Water Adjusted Vegetation Index  
255 (WAVI). These two new versions were found more sensitive to seagrass LAI and percentage cover density, and  
256 discriminated better among species of seagrass (Yang and Yang, 2009; Villa et al., 2013). To separate and map  
257 vegetation features over some lake ecosystems in Italy, the NDAVI and the WAVI performed suitably (Villa et al.,

258 2014). As well, for open water features delineation, Mcfeeters (1996) replaced the difference between “NIR and red”  
259 in the NDVI with that between “green and NIR”, and he baptised this new combination the Normalized Difference  
260 Water Index (NDWI). In Taihu and Duck Lakes in China, NDVI and NDWI were used for wetland and SAV pattern  
261 delineation and classification (Lin et al., 2010; Zhao et al., 2013). Likewise, the visible atmospherically resistant index  
262 (VARI) was proposed by Gitelson et al. (2002a) to estimate the green vegetation fraction. While the triangular  
263 greenness index (TGI) was developed by Hunt et al. (2013) based on the chlorophyll absorption features. The  
264 capability of VARI and TGI was examined by Li (2018) who highlighted the advantage of VARI compared to TGI  
265 for seagrass biomass mapping in Core Banks in North Carolina in the USA. Proposed by Richardson and Wiegand  
266 (1977), the difference vegetation index (DVI) provided satisfactory results for mangrove cover and carbon stock  
267 estimation in the estuary and marine environment (Candra et al., 2016). Moreover, the difference-index between the  
268 blue and the green bands (DIF-BG) showed the best fits between observed and predicted SAV as reported by Mumby  
269 et al. (1997).

270

271

[ Figure 1 ]

### 272 3. Materials and Methods

273 Fig. 2 illustrates the followed methodology, which is based on a field survey to collect samples including seawater,  
274 sediments, seagrass (*Halodule uninervis* and *Halophila stipulacea*) and algae (green and brown) from shallow marine  
275 environment at different depths (0.50 to 7 m) off southeast Bahrain Island. To simulate the marine environment, an  
276 experimental mode was established in a Goniometric-Laboratory and spectral measurements were performed using  
277 an Analytical Spectral Devices (ASD) spectroradiometer over each separate and mixed species at different coverage  
278 rate (0, 10, 30, 75, and 100%), as well as simulating the seabed with dark and bright colors. To assess the spectral  
279 signatures variability that can be found among each separate or mixed species at varying coverage rates, all measured  
280 spectra were analyzed and transformed using continuum-removed reflectance spectral (CRRS) approach (see section  
281 3.4). Then, the spectra were resampled and convolved in the solar-reflective spectral bands of MSI and OLI sensors  
282 using the *Canadian Modified Simulation of a Satellite Signal in the Solar Spectrum* (CAM5S) (Teillet and Santer,  
283 1991) based on Herman radiative transfer code (RTC), and the relative spectral response profiles characterizing the  
284 filters of each instrument in the VNIR bands. Afterward, convolved spectra were converted into several WVI  
285 integrating the red, green, and blue bands. For comparison and sensor differences quantification, statistical fits were  
286 conducted using linear regression analysis ( $p < 0.05$ ) between reflectances in homologous bands and between the  
287 examined homologous WVI derived from the two sensors data considering all samples, i.e., seawater, sediments,  
288 seagrass, and algae species (individually and mixed at the considered coverage rates). The coefficient of determination  
289 ( $R^2$ ), difference values, and root mean square difference (RMSD) were calculated for reflectances and all versions of  
290 investigated WVI's.

291

292

[ Figure 2 ]



### 293 3.1. Study Site

294 The area under investigation in this research is the water boundary of the Kingdom of Bahrain (25° 32' to 26°00'N,  
295 50° 20' to 50° 50'E) which is a group of islands located in the Arabian Gulf, east of Saudi Arabia and west of Qatar  
296 (Fig. 3). The archipelago comprises 33 islands, with a total area of 8269 km<sup>2</sup>, 9% of it is a land area (778.4 km<sup>2</sup>).  
297 Along the southeast coast of Bahrain, the continental plateau extends for kilometers with a depth of less than one or  
298 two meters. The main island of Bahrain is surrounded by shoal areas named “Fashts” where depths do not exceed 10  
299 m (Bannar i and Kadhem, 2018). These areas generally support a variety of species of seagrass, algae, coral, and  
300 fishes. Moreover, they play an important role in the hydrodynamic regime, which supports diverse biological  
301 ecosystems. Fig. 3 also illustrates the reclamation and dredging operations that have occurred in the study area over  
302 the past three decades where several coastal developmental projects are constructed, and others are in progress. These  
303 anthropogenic activities strongly contribute to the degradation and even to the destruction of seagrass species and  
304 associated coastal ecosystems.

305

306

[ Figure 3 ]

### 307 3.2. Field sampling

308 Seagrass and algae samples were collected on 4<sup>th</sup> May 2017 from different meadows locations, which are characterized  
309 by a depth range from 0.5 to 7 m in the south and southeast waters of Bahrain (Fig. 4a). Some locations were dominated  
310 with *Halodule uninervis* (HU), others scattered, and others were densely mixed between HU and *Halophila stipulacea*  
311 (HS). HU is the most dominant species (Fig. 4b), it occurs as dense or scattered meadows patches along shoreline  
312 (Erfteimeijer and Shail, 2012). This species is like grass with narrow leaves (around 3 mm in width and 25 cm in  
313 length). Whereas, HS (Fig. 4c) has darker green leaves reaching 10 cm in length and it is widely present in the Arabian  
314 Gulf. The brown (BA, Fig. 4d) and green (GA, Fig. 4e) algae were accessible near to shores and shallow water in  
315 general. In addition to the sediments (Fig. 4f) and pure seawater samples, which were collected separately, samples  
316 of each seagrass and algae species were selected and harvested in healthy and fresh conditions from several stations  
317 within the study area. Then, they were stored separately in non-translucent plastic bags with seawater and immediately  
318 placed in a cooler for transportation from the field to the laboratory. This was done to prevent structural and leaf  
319 pigment damages due to the delay between sampling time and spectroradiometric measurements in the Goniometric-  
320 Laboratory.

321

322

[ Figure 4 ]

### 323 3.3. Spectroradiometric measurements

324 Spectroradiometric measurements were acquired in a dark BRDF Goniometric-Laboratory above each sample  
325 separately, then above mixed samples (Fig. 5), using an ASD spectroradiometer (ASD Inc., 2015). This instrument is  
326 equipped with two detectors operating in the VNIR and shortwave-infrared (SWIR), between 350 and 2500 nm. It  
327 acquires a continuous spectrum with a 1.4 nm sampling interval from 350 to 1000 nm and 2 nm from 1000 to 2500

328 nm. The ASD resamples the measurements in 1-nm intervals, which allows the acquisition of 2151 contiguous  
329 hyperspectral bands per spectrum. The sensor is characterized by the programming capacity of the integration time,  
330 which allows an increase of the SNR and stability. The data were acquired at nadir with a field of view (FOV) of 25°  
331 and a solar zenith angle of approximately 5° by averaging 40 measurements. The ASD was installed on a BRDF  
332 Goniometric-System with a height of approximately 65 cm over the target, which makes it possible to observe a  
333 surface of ~ 830 cm<sup>2</sup>. A laser beam was used to locate the center of the ASD-FOV. The reflectance factor of each  
334 sample was calculated as the ratio of target radiance to the radiance obtained from a calibrated “Spectralon panel”  
335 according to the method described by Jackson et al. (1980). Moreover, the corrections were applied for the wavelength  
336 dependence and non-Lambertian (i.e. uneven light distribution in all directions) behavior of the panel (Sandmeier et  
337 al., 1998; ASD, 2015; Ben-Dor et al., 2015). The measurements were carried out above each collected sample  
338 including seawater, sediments, seagrass, and algae species as well as mixed species (seagrass and algae) considering  
339 different coverage rates (0, 10, 30, 75, and 100%). Each sample was placed and measured twice in black and bright  
340 (yellow) large bowls, considering two sedimentary substrates (dark and bright) underlying the seagrass and algae  
341 samples that were submerged by seawater, i.e., simulating the aquatic environment. Since the remote sensing of  
342 benthic aquatic vegetation is mostly limited to the VNIR ranges (Fig. 1) only the wavelengths interval between 400  
343 and 1000 nm are considered in our analyses.

344

345

[ Figure 5 ]

#### 346 **3.4. Continuum-removed reflectance spectral (CRRS) transformation**

347 Spectral signatures are processed and transformed using numerous approaches to retrieve information about change  
348 in absorption features (position, depth, width, and asymmetry) of a particular target over a specific bandwidth between  
349 350 and 2500 nm (Van-Der-Meera, 2004). To emphasize these absorption features, many approaches were proposed  
350 including relative absorption-band-depth (Crowley et al., 1989), spectral feature fitting technique, and Tricorder and  
351 Tetracorder algorithms (Clark et al., 2003). These approaches work on the so-called CRRS approach, thus recognizing  
352 that the absorption in a spectrum has a continuum and individual absorption features (Clark *et al.*, 1987; Van-Der-  
353 Meera, 2004; Clark *et al.*, 2014). Proposed by Clark and Roush (1984), CRRS transformation and analysis allows the  
354 isolation of individual absorption features in the hyperspectral signature of a specific target under investigation,  
355 analysis, and comparison. It normalizes the original spectra and helps to compare individual absorption features from  
356 a common baseline (Clark *et al.*, 1987). The continuum is a convex hull fit over the top of a spectrum under study  
357 using straight-line segments that connect local spectra maxima. The first and last spectral data values are on the hull;  
358 therefore, the first and last bands in the output continuum-removed data file are equal to 1.0. In other words, after the  
359 continuum is removed, a part of the spectrum without absorption features will have a value of 1, whereas complete  
360 absorption would be near to 0, and with most absorptions falling somewhere in between. The CRRS approach was  
361 used for discriminating and mapping rocks mineralogy (Clark et al., 1990; Clark and Swayze, 1995), land vegetation  
362 cover (Kokaly et al., 2003; Huang et al., 2004; Manevski et al., 2011), and seagrass and SAV (Barillé et al., 2011;

363 Bargain et al., 2012; Wicaksono et al., 2019; Indayani et al., 2020). In this study, the continuum algorithm  
364 implemented in the ENVI image processing system was used (ENVI, 2012).

### 365 **3.5. Spectral sampling and convolving in MSI and OLI spectral bands**

366 Since 1972, the Landsat scientific collaboration program between NASA and USGS constitutes the continuous record  
367 of the Earth's surface reflectivity from space. Indeed, the Landsat satellites series support five decades of a global  
368 medium spatial resolution data collection, distribution, and archive of the Earth's surfaces (Bannari et al., 2004;  
369 Loveland and Dwyer, 2012) to support research, applications, and climate change impacts analysis at the global, the  
370 regional and the local scales (Roy et al., 2014 and 2016; Wulder et al., 2015). Benefiting from the acquired space-  
371 engineering experience, from the heritage of Landsat instruments, and the advanced development of technology during  
372 the last five decades, the fourth generation of Landsat is composed of two similar sensors with very high spectral and  
373 radiometric sensitivities: OLI-1 and OLI-2 (Markham et al., 2016; Li and Chen, 2020). The OLI-1 carried onboard  
374 Landsat-8 was launched on 11<sup>th</sup> February 2013, and OLI-2 onboard Landsat-9 was launched on 27<sup>th</sup> September 2021  
375 (NASA, 2019 and 2021). The OLI sensors collect land-surface reflectivity in the VNIR, SWIR, and panchromatic  
376 wavelength with a FOV of 15° covering a swath of 185 km with 16 days' time repetition at the equator. The band  
377 passes are narrower to minimize atmospheric absorption features (NASA, 2014), especially the NIR spectral band  
378 (0.865 µm). Two new spectral bands have been added: a deep blue visible shorter wavelength (band 1: 0.433 - 0.453  
379 µm) designed specifically for water resources and coastal zone investigation and a new SWIR band (9: 1.360 - 1.390  
380 µm) for the detection of cirrus clouds. Moreover, compared to previous TM and ETM+ sensors using only 8 bit, the  
381 OLI design results in more sensitive instruments with a significant improvement of the SNR radiometric performance  
382 quantized over a 12-bit dynamic range (Level 1 data), and raw data are delivered in 16 bit. The high performance of  
383 SNR associated with improved radiometric and spectral resolutions provide a superior dynamic range of radiance by  
384 reducing saturation problems and, therefore, enabling better characterization of land and water surface conditions  
385 (Knight and Kvaran, 2014), especially with orbit reflective radiometric calibration better than 3% (Markham et al.,  
386 2014; Gascon et al., 2017). Table 1 summarizes the effective bandwidth characteristics of OLI-1 and OLI-2 sensors.

387  
388 [ Table 1 ]  
389

390 Otherwise, the Sentinel-2 mission is the result of close collaboration between the European Space Agency, the  
391 European Commission, industry, service providers, and data users. It is composed of two satellites, Sentinel 2A and  
392 2B that were launched in June 2015 and in March 2017, respectively. Both satellites are equipped with identical MSI  
393 sensors to provide continuity to the SPOT missions and to improve the Landsat-OLI temporal frequency (Drusch et  
394 al., 2012). The synergy between the four sensors (MSI-2A, MSI-2B, OLI-1, and OLI-2) significantly increase the  
395 temporal resolution (around 2 days) offering new opportunities for several environmental and natural resource  
396 applications, such as the vigour of vegetation cover, emergency management, water quality, seagrass meadows, and  
397 climate change impacts analysis at local, regional, and global scales. The MSI images the Earth's surface reflectivity  
398 with a large FOV (20.6°) in 13 spectral bands with several spatial resolutions from 10 to 60-m; four bands with 10-m

399 (blue, green, red, and NIR-1), six bands with 20-m (Red-Edge, NIR-2, and SWIR), and three bands with 60-m (coastal,  
 400 water vapor and cirrus). The swath of each scene is 290 km, permitting global coverage of the Earth's surface every  
 401 10 days. The MSI radiometric performance is coded in 12 bits, ensuring radiometric calibration accuracy of better  
 402 than 3% and an excellent SNR (Markham et al., 2014; Li et al., 2017). Table 1 summarizes the effective bandwidth  
 403 characteristics of MSI-2A and MSI-2B sensors.

404 As discussed above, the measured bidirectional reflectance factors with the ASD have a 1-nm interval allowing  
 405 the acquisition of 2151 contiguous hyperspectral bands per spectrum. However, most multispectral remote sensing  
 406 instruments measure integrated reflectance over broad bands (equation 1). Consequently, the average of 40 spectra  
 407 measured with the ASD over each sample was resampled and convolved to match the solar-reflective spectral  
 408 responses functions characterizing the optics and electronics of MSI and OLI instruments in the VNIR spectral bands  
 409 (Fig. 6). In this step, the resampling procedure considers the nominal width of each spectral band (Table 1). Then, the  
 410 convolution process was executed using the CAM5S transfer radiative code (Teillet and Santer, 1991). This  
 411 fundamental step simulates the signal received by the considered sensors at the top of the atmosphere from a surface  
 412 reflecting solar and sky irradiance at sea level, considering the filter of each band (Fig. 6), and assuming ideal  
 413 atmospheric conditions without scattering or absorption (Zhang and Roy, 2016). Accordingly, the equivalent  
 414 convolved reflectance ( $\rho(\lambda_i, \lambda_s)_i$ ) over each sample was generated at the satellite orbit altitude in homologous VNIR  
 415 spectral bands of each sensor (Slater, 1980):

$$417 \quad \rho(\lambda_i, \lambda_s)_i = \frac{\int_{\lambda_i}^{\lambda_s} R(\lambda) \cdot S(\lambda)_i \cdot d(\lambda)}{\int_{\lambda_i}^{\lambda_s} S(\lambda)_i \cdot d(\lambda)} \quad (1)$$

418  
 419 Where  $\rho(\lambda_i, \lambda_s)_i$  is the equivalent convolved reflectance of the band "i" of each sensor,  $\lambda_i$  to  $\lambda_s$  are the spectral  
 420 wavelength ranges of the band "i" of each sensor,  $R(\lambda)$  is the corresponding reflectance at wavelength " $\lambda$ " measured  
 421 by the ASD, and  $S(\lambda)_i$  is the corresponding spectral responsivity value of the spectral response function of the band  
 422 "i" of each sensor (Fig. 6). It is important to note that the MSI-NIR-2 broadband (band-8: 785 - 900 nm) is not  
 423 considered in this study because it is not a real homologous band of OLI-NIR, and it has a greatest reflective band  
 424 difference with the OLI-NIR (851–879 nm). The OLI-NIR spectral response function intersects with only 20% of the  
 425 MSI-NIR-2 response function. Moreover, the MSI red-edge bands were not considered as they are not acquired by the  
 426 OLI sensor.

427

428

[ Figure 6 ]

### 429 3.6. Data Processing

430 In addition to remote sensing sensor technologies' improvement and innovation, a variety of processing methods have  
 431 been applied for spectral data for mapping and monitoring seagrass and habitats in shallow coastal waters. They were  
 432 applied to highlight the seagrass and algae species composition, leaf area index estimation, percentage cover mapping,

433 etc. They include matched filtering approach (Li et al., 2012), object-based image analysis (Roelfsema *et al.*, 2014),  
 434 adaptive coherence estimator and constrained energy minimization (Li et al., 2012), artificial neural network model  
 435 (Perez et al., 2020), linear spectral mixture analysis (Uhrin and Townsend, 2016; Chen et al., 2016), spectral angle  
 436 mapper (Peneva et al., 2008; Li et al., 2012; Marcello et al., 2018; Wicaksono et al., 2019), classification tree analysis  
 437 (Wicaksono et al., 2019), random forest (Bayyana et al., 2020), support vector machines (Marcello et al., 2018;  
 438 Bakirman and Gumusay, 2020; Perez et al., 2020; Bayyana et al., 2020), and machine learning regression (Traganos,  
 439 2020; Bakirman and Gumusay, 2020). Undeniably, these sophisticated and complicated methods require extensive  
 440 training information and field endmember measurements. However, the simplicity of empirical and semi-empirical  
 441 methods based on vegetation indices are easier to transfer between sensors and can be used as a robust alternative  
 442 compared to the complex processing methods; because these methods are based on the knowledge of spectral  
 443 absorption features that characterize specifically the target under investigation. Moreover, these methods have the  
 444 advantage of being reproducible, easily transferable, and applicable in other geographic regions. Each method has  
 445 advantages and limitations, especially in shallow water. In this study, after the spectral analysis and CRRS  
 446 transformation, the capability and comparison of the VNIR homologous spectral bands of MSI and OLI sensors were  
 447 investigated for seawater, sediments, seagrass, algae, and mixed species discrimination at different coverage rates.  
 448 Then, although the literature refers to more than fifty vegetation indices for land vegetation cover monitoring and  
 449 characterization (Bannari et al., 1995), only the most popular indices that have been used for seagrass and SAV in  
 450 different marine environments around the world were retained in this study. After spectral data pre-processing,  
 451 sampling, and convolving, the indices TGI, VARI, and Diff(G-B) were implemented and tested respecting their  
 452 original equations. While the NDVI, SAVI, EVI, TDVI, NDWI, and DVI indices were calculated in three versions by  
 453 integrating the red, blue, and green bands. The equations of the considered indices are as follow:

454

$$455 \quad \text{NDVI} = (\rho_{\text{NIR}} - \rho_{\text{Red}}) / (\rho_{\text{NIR}} + \rho_{\text{Red}}) \quad (\text{Rouse et al., 1974}) \quad (2)$$

$$456 \quad \text{SAVI} = 1.5 * (\rho_{\text{NIR}} - \rho_{\text{Red}}) / (\rho_{\text{NIR}} + \rho_{\text{Red}} + 0.5) \quad (\text{Huete, 1988}) \quad (3)$$

$$457 \quad \text{TDVI} = 1.5 * (\rho_{\text{NIR}} - \rho_{\text{Red}}) / (\sqrt{(\rho_{\text{NIR}}^2 + \rho_{\text{Red}} + 0.5)}) \quad (\text{Bannari et al., 2002}) \quad (4)$$

$$458 \quad \text{NDWI} = (\rho_{\text{Green}} - \rho_{\text{NIR}}) / (\rho_{\text{Green}} + \rho_{\text{NIR}}) \quad (\text{McFeeters, 1996}) \quad (5)$$

$$459 \quad \text{EVI} = 2.5 * (\rho_{\text{NIR}} - \rho_{\text{Red}}) / (\rho_{\text{NIR}} + 6 * \rho_{\text{Red}} - 7.5 * \rho_{\text{Blue}} + 1) \quad (\text{Huete et al., 2002}) \quad (6)$$

$$460 \quad \text{DVI} = \rho_{\text{NIR}} - \rho_{\text{Red}} \quad (\text{Richardson and Wiegand, 1977}) \quad (7)$$

$$461 \quad \text{VARI} = (\rho_{\text{Green}} - \rho_{\text{Red}}) / (\rho_{\text{Green}} + \rho_{\text{Red}} - \rho_{\text{Blue}}) \quad (\text{Gitelson et al., 2002a}) \quad (8)$$

$$462 \quad \text{TGI} = \rho_{\text{Green}} - 0.39 * \rho_{\text{Red}} - 0.61 * \rho_{\text{Blue}} \quad (\text{Hunt et al., 2013}) \quad (9)$$

$$463 \quad \text{Diff(G-B)} = \rho_{\text{Blue}} - \rho_{\text{Green}} \quad (\text{Mumby et al., 1997}) \quad (10)$$

464

465 The wavelength ranges of the used VNIR bands for Sentinel-MSI and Landsat-OLI are summarize in Table 1.

### 466 3.7. Statistical analyses

467 As discussed previously, the respective MSI and OLI spectral response profiles characterizing the filters of each  
 468 spectral band differ somewhat (Fig. 6). To examine the impact of this difference, statistical analyses were computed

469 using “Statistica” software. The relationships between the product values (reflectances and WVI’s) derived from MSI  
 470 against those obtained from OLI were analyzed between homologous bands using a linear regression model ( $p < 0.05$ ).  
 471 As well, the  $R^2$  was used to evaluate the strength of this linear relationship. For this process, the resampled and  
 472 convolved spectra of all samples’ reflectance data were used, and the homologous values in VNIR bands of MSI and  
 473 OLI were compared using the 1:1 line. Ideally, these independent variable values should have a correspondence of  
 474 1:1. Additionally, the root mean square difference (RMSD) between both sensors was derived (Willmott, 1982; Zhang  
 475 et al., 2018):

$$476 \quad \text{RMSD} = \sqrt{\frac{\sum_i^n (v_i^{OLI} - v_i^{MSI})^2}{n}} \quad (11)$$

478  
 479 Where RMSD is between corresponding Landsat-OLI and Sentinel-MSI variables values (reflectances and WVI’s),  
 480 “ $v_i$ ” is the variable under analysis and “ $i$ ” is its index ( $i = 1$  to  $n$ ).

## 481 **4. Results analysis**

### 482 **4.1. Spectral and CRRS analysis**

483 Spectral signatures of seagrass and algae species are measured separately and mixed in black and yellow large bowls  
 484 using two sedimentary substrates (dark and bright). They are presented separately for the examined coverage rates,  
 485 namely 10, 30, 75, and 100% (Fig. 7, a-d). Overall, the reflectance signatures of seagrass and algae samples are similar  
 486 to those of healthy vegetation canopy. These reflectance signatures exhibit slight absorption features near 450 nm and  
 487 others stronger between 650 and 700 nm with a minimum at 670 nm caused by the chlorophyll; as well as a significant  
 488 reflection between 520 and 600 nm due to carotenoid pigments and high reflectance in the NIR attributed to internal  
 489 tissue structure (700 to 900 nm). Differently to land vegetation, the red-edge is not well developed (very weak)  
 490 particularly for non-dense seagrass and algae due to high red and NIR absorption by water molecules as shown in Fig.  
 491 1. Generally, absorption or reflection of pigmentations between species occurs in different wavelengths but the  
 492 strength of absorption gradually increases in the red as the coverage rate increases.

493 For scattered and low coverage (~ 10 %), the shapes of all spectra are similar, without the possibility to identify  
 494 specific absorption features or to separate among species according to their spectra in the visible domain (Fig. 7a).  
 495 The highest reflectance values vary between 10% and 15% across NIR wavelengths, and a difference reflectance  
 496 ( $\Delta\rho_{\text{NIR}}$ ) around 5%, while in the visible all the reflectance values are below 5% with  $\Delta\rho_{\text{visible}}$  are also  $< 5\%$ . For this  
 497 low and sparse cover, it is observed that the reflectance is influenced by spectral properties of the underlying  
 498 sediments, fragments of vegetation, light shading, etc., thus contributing to the confusion between spectral signatures.  
 499 Definitely, under such conditions, it is a challenge to distinguish between seagrass and/or algae species based only on  
 500 their spectral signatures. Whereas, the measurements acquired over somewhat denser coverage rates (~ 30 %) show  
 501 analogous spectral behaviour and patterns with overlap among spectra in visible wavelengths (400 to 700 nm), but a  
 502 slight separability between species is relatively apparent in NIR (Fig. 7b).

503 Furthermore, unlike scattered or less dense cover ( $\leq 30\%$ ), the analysis of the dense and very dense coverage rates  
504 (75 and 100%) showed that the optical properties (darkness or brightness) of the underlying substrate does not have a  
505 significant effect on the measured spectra. For these coverage ranges, the clear and normal behaviour of vegetation  
506 cover spectra are observed. The absorption feature is weak in the blue (450–480 nm) but more accentuated in red (670  
507 nm), the reflection peak is more highlighted in green (550 nm), and the reflectance values increase notably and  
508 gradually in NIR with the increase of the coverage rate. Although the seagrass has a distinct spectral response  
509 compared to the algae, especially in the green and NIR regions of the spectrum, significant spectral differences are  
510 noted for the HU with the highest reflectance, followed by GA, HS, and BA. This order is probably controlled by the  
511 leaves structures that are specific for each type of seagrass or algae. The reflectance values in the visible are controlled  
512 by the absorption of chlorophyll pigmentations in blue and red wavelengths, and by the carotenoid pigmentations in  
513 the green band. In addition, compared to HS and BA spectra, HU and GA showed relatively strong absorption by  
514 chlorophyll in red wavelengths. This difference is due to the nature of chlorophyll in each species. Indeed, brown  
515 algae contain accessory pigments “fucoxanthin” and chlorophyll “c” (Johnsen and Sakshaug, 2007), while seagrass  
516 are flowering plants, and their leaves contain chlorophyll “b” (Cummings and Zimmerman, 2003). It is observed also  
517 that the BA carotenoid pigments (fucoxanthin) are characterized by spectral features at 630 and 650 nm that are not  
518 present in the spectra of HS, HU, and GA (Fig. 7). However, despite all these spectral characteristics the difference in  
519 reflectance values among all species (individual and mixed) is  $\leq 6\%$  in the visible and  $\leq 13\%$  in NIR for a very dense  
520 cover (100%). Therefore, these results suggest that it is probably possible for the blue, green, and NIR wavelengths  
521 to discriminate among the considered seagrass and algae species if they are homogeneous with high or very high  
522 densities.

523 Otherwise, the CRRS transformations are presented in Fig. 7 (e-h) with Sentinel-MSI relative spectral response  
524 profiles characterizing the filters of VNIR bands. The lower CRRS values indicate the greatest potential spectral  
525 separability, which means the identification of the appropriate wavelengths to discriminate among the considered  
526 classes of investigated species. As shown in Fig. 7 (e-h), the CRRS significantly enhances the spectral separability  
527 among the seagrass and algae classes, especially in the visible bands. Two main absorption features are highlighted in  
528 the blue (485–498 nm) and red ( $\sim 670$  nm) regardless the species. In the green, one major reflection peak is observed  
529 around 544 nm for HU and GA, one around 530 nm for HS, and three peaks are well distinguished for BA at 578,  
530 595, and 640 nm (Fig. 7h). These differentiation features become clearer as the coverage rates increase especially in  
531 blue and NIR wavelengths. For a low coverage rate ( $\sim 10\%$ ), the strongest absorption depth is that of GA (0.46)  
532 followed by HU (0.58), HS (0.74), and BA (0.78) in the blue (Fig. 7e). While in the red, CRRS pointed out that  
533 regardless of the coverage rate, a strong similarity is observed between HU and GA due to their high content of  
534 chlorophyll pigmentation with a depth of absorption around 0.29, followed by HS and BA that are characterized by  
535 less absorption depth ( $\sim 0.50$ ). In these two waveband domains (blue and red), the absorption features become deeper  
536 with increasing coverage density. Likewise, when the cover rate of all species becomes denser (100%), similar  
537 absorption characteristics are exhibited in the red band between HU and GA species; as well as between HS and BA  
538 (Fig. 7h). While in the blue and NIR wavelengths, the CRRS highlights the distinction and differentiation between  
539 species. On the other hand, as the coverage increases from 10 to 100%, the reflection peak in the green waveband

540 becomes less pronounced due to the high content of carotenoid pigment; also a strong similarity is observed between  
541 HU and GA. Moreover, the curves of CRRS of the mixed species occupy an intermediate position of absorption  
542 features between the homogeneous samples and, therefore, the differentiation between absorption characteristics  
543 becomes very slight. Accordingly, the discrimination between pure and mixed species becomes very difficult or even  
544 impossible. Overall, spectral and CRRS analyses highlighted the importance of the blue, green, and NIR wavelengths  
545 for seagrass and algae detection and probable discrimination based on hyperspectral measurements. These results  
546 corroborate the physical concept presented in Fig. 1 that the blue and green electromagnetic radiation penetrates a  
547 deeper vertical column of water. While despite its limited penetration, the NIR shows a certain sensitivity to the  
548 biomass density and its spatial distribution.

549

550

[ Figure 7 ]

#### 551 4.2. Resampling and convolving in OLI and MSI bands

552 Fig. 8 illustrates the scatter-plots between the resampled and convolved reflectance values in the VNIR homologous  
553 bands of the MSI and OLI sensors. Simulated at the top of the atmosphere using all considered samples (seawater,  
554 sediments, seagrass, algae and mixed species of both seagrass and algae at varied coverage rates), they allow the  
555 analysis of the difference in reflectance values ( $\Delta\rho$ ) and RMSD due exclusively to dissimilarities in spectral response  
556 function between homologous bands. These scatter-plots reveal a near-perfect fit with 1:1 line expressing an excellent  
557 coefficient of determination ( $R^2$  of 0.999) between homologous bands with the slopes and intercepts very near to unity  
558 and zero, respectively. Thus, the derived  $\Delta\rho$  values are null for VNIR homologous bands for seawater and are  
559 insignificant for dark and bright substrate sediments in all bands (i.e., 0.009 for green and 0.002 for the coastal, blue,  
560 red, and NIR bands). While, for seagrass and algae (HS, HU, GA, and BA),  $\Delta\rho$  vary between 0.003 and 0.02 regardless  
561 of the coverage rate or the considered spectral band. Moreover, the achieved overall RMSD in reflectance between  
562 MSI and OLI homologous bands considering all samples are insignificant ( $\leq 0.0015$ ) for blue, green, and red bands,  
563 and null for coastal and NIR bands. It is also observed that all the bands are insensitive to the variation of the colors  
564 of the bowls and the sedimentary substrate optical properties. These results pointed out that MSI and OLI sensors are  
565 spectrally similar and can be used jointly for high temporal frequency to monitor seagrass and algae dynamics in time  
566 and space. Therefore, due to this near-perfect spectral similarity between these instruments, our analysis in the  
567 following sections will focus only on the MSI sensor.

568

569

[ Figure 8 ]

570

571 Fig. 9 illustrates the reflectances of seagrass, algae, and seawater resampled and convolved in VNIR bands of MSI or  
572 OLI sensors considering each species separately and all species at different coverage rates. Compared to the measured  
573 hyperspectral signatures (Fig. 7), these broadband spectra are more generalized and less precise because these spectra  
574 lost the specific and unique absorption features of seagrass and/or algae species caused by pigmentations as discussed  
575 above. However, such broadband spectra retain the same spectral pattern as the original spectra. Regardless of the



576 species, the graphics summarized in Fig. 9 exhibit similar shape and pattern, but with a slight difference in reflectance  
 577 values between species in the visible bands. If we consider the species separately (HS, HU, GA, and BA) in different  
 578 coverage rates (10, 25, 75, and 100%), the reflectance difference values ( $\Delta\rho$ ) are  $\leq 0.02$ ; and insignificant ( $\Delta\rho \leq 0.002$ )  
 579 for pure seawater and sediments in all VNIR bands. Hence, these species are not spectrally distinguishable particularly  
 580 in the visible whatever the coverage. While, if we consider all samples (seagrass, algae, and mixed) in all coverage  
 581 rates (Fig. 9e), the  $\Delta\rho$  are equal to 0.03 in coastal and blue bands, 0.05 in green, 0.035 in red and 0.21 in NIR. Except  
 582 for the NIR, the calculated  $\Delta\rho$  values in the visible are approximately identical to the accuracies achieved from  
 583 radiometric calibration and atmospheric corrections. Therefore, relying on the multispectral bandwidth of OLI and  
 584 MSI sensors, it is difficult or even impossible to differentiate or to map seagrass and algae individually at the species  
 585 level. Accordingly, SAV classes' discrimination and mapping will be discussed.

586

587 [ Figure 9 ]

588 **4.3. Vegetation indices analysis**

589 In this third part, the NDVI, SAVI, EVI, TDVI, NDWI, and DVI indices were implemented and analysed in three  
 590 versions each by integrating the red, blue, and green bands; while the indices TGI, VARI, and Diff(G-B) were  
 591 calculated and tested respecting their original equations. In total, 21 combinations of indices were calculated for each  
 592 sensor. The statistical analyses ( $p < 0.05$ ) focus on the similarity or dissimilarity between MSI and OLI homologous  
 593 indices, and their potential for seagrass and algae discrimination. Except for the TGI and VARI indices, the results  
 594 revealed an excellent linear relationship ( $R^2$  of 0.999) between MSI and OLI products regardless of the compared  
 595 index and the integrated spectral bands (red, green, and blue). Overall, the scatter-plots presented in Fig. 10 depict a  
 596 very good fit to the 1:1 line with the slopes and intercepts very near to unity and zero, respectively. However, despite  
 597 its near-perfect linearity and insignificant RMSD between MSI and OLI values (0.001), the TGI show a very weak  
 598 and limited spatial variability with a range between 0.0 for pure seawater and 0.05 for a very dense coverage (100%)  
 599 of seagrass or algae (Fig. 10e). This range cannot allow the differentiation among the marine environment classes,  
 600 because this index was not developed for biomass sensing but was designed for crop nitrogen requirements detection.  
 601 Likewise, although the scatter-plot of VARI shows an excellent coefficient of determination ( $R^2$  of 0.99), estimates  
 602 of this index with the MSI sensor exceed those from OLI, resulting in the data not fitting the 1:1 line very well (Fig.  
 603 10f). Moreover, the difference values of VARI derived from MSI and OLI data vary between 0.0 and 0.14 depending  
 604 on the sample species and its coverage rate, with an overall RMSD of 0.03. This result can be explained by the fact  
 605 that the VARI uses only the visible ranges of the spectrum and does not consider the NIR band, which is the most  
 606 informative about the biomass density. In addition, it was developed particularly for very dense (100%) wheat crops;  
 607 moreover, it was designed principally for coarse data acquired by the SeaWiFS, MODIS, MISR, and MERIS sensors.  
 608 According to Gitelson et al. (2002b), many factors potentially decrease the accuracy of the VARI (e.g. vegetation  
 609 cover species, canopy architecture, and sun illumination geometry). For wheat and corn species, this index yielded  
 610 RMSE of around 10% (Gitelson et al., 2002a). Therefore, the weaknesses raised for these two indices (TGI and VARI)  
 611 are not caused by the impact due exclusively to the dissimilarities in spectral response function between homologous

612 bands of MSI and OLI sensors, but due to their mathematical concepts that are intended for a single and specific  
613 application.

614 Furthermore, the scatter-plots presented in Fig. 10 (a-d) are showing examples of certain indices including NDWI,  
615 WAVI, WEVI, and WTDVI. Overall, the indices are fitting very well the 1:1 line with  $R^2$  of 0.99, slopes very near to  
616 unity and intercepts to zero. The indices show that the derived WVI from MSI and OLI data give similar estimates of  
617 seagrass and algae species in a shallow marine environment. Considering all investigated samples in this study, the  
618 interval difference values between homologous indices vary between 0.0 and 0.01 for all versions of WTDVI, WAVI,  
619 WTDVI, and Diff(G-B); while they vary between 0.0 and 0.04 for NDWI, WEVI and NDWI. These differences values  
620 are satisfactory and remain equal to or less than the combined inaccuracies of atmospheric corrections and sensor  
621 radiometric calibration. Moreover, the achieved RMSD values between MSI and OLI homologous indices are  
622 insignificant ( $RMSD \leq 0.01$ ) for all indices (Table 2) regardless of the integrated spectral band. These analyses pointed  
623 out that MSI and OLI sensors can be combined for high temporal frequency to monitor the dynamic of biophysical  
624 products in time and space in a shallow marine environment.

625

626 [ Table 2 ]

627

628 [ Figure 10 ]

629

630 Fig. 11 summarises the linear regressions ( $p < 0.05$ ) between the best indices and the reflectances in NIR considering  
631 all samples, i.e., seawater, sediments, seagrass, algae, and mixed species classes with different coverage rates (10, 30,  
632 75, and 100%). The computed indices (NDVI, SAVI, EVI, TDVI, NDWI, and DVI) with the blue, green, and red  
633 bands are the most relevant for SAV differentiation and mapping. Firstly, it is observed that the indices NDVI and  
634 NDWI provided similar results with opposite signs, i.e., symmetrically opposed concerning the X-axis. Indeed,  
635 whatever the integrated band, the NDWI results are always symmetrical compared to those of NDVI but with negative  
636 values. However, such results are not showing the truth because negative values are automatically reset to zero by the  
637 image processing system and, therefore, it is probable that the results will be inaccurate. Furthermore, when the red  
638 and blue bands are implemented in the NDVI equation, insignificant fits ( $R^2$  of 0.40) were achieved. Whereas,  
639 improved results are obtained with the integration of the green band ( $R^2$  of 0.63) and the index is named NDWVI.  
640 Analogous results are obtained by Diff(G-B) and VARI indices with  $R^2$  of 0.63 (Table 2) when all samples are  
641 considered. Luckily, the statistical fits of these three indices (NDWVI, Diff(G-B), and VARI) becomes significantly  
642 improved when unique species is considered, such as only seagrass or only algae ( $R^2$  of 0.85). Whereas, in addition  
643 to its weakness and limited sensitivity to the spatial variability of seagrass and algae, the TGI was irrelevant for SAV  
644 discrimination yielding a very low fits ( $R^2$  of 0.20) whatever the considered species.

645

646 [ Figure 11 ]

647

648 As discussed previously, when integrating the blue and green bands, the indices WDVI, WAVI, WEVI, and  
649 WTDVI outperformed all examined indices regardless of the species (seagrass, algae, or mixed), yielding a very  
650 significant coefficient of determination for mixed species ( $0.89 \leq R^2 \leq 0.96$ ) (Fig. 11 a-d, and Table 2). Calculated  
651 with blue, green, or red bands, the DVI (noted WDVI) discriminated among SAV classes significantly ( $R^2 \leq 0.92$ ),  
652 but it underestimates the SAV as shown in Fig. 10-d. However, WAVI, WEVI, and WTDVI offer similar trends  
653 regardless the considered species ( $R^2 \leq 0.92$  for mixed or seagrass only, and  $R^2$  of 0.82 for algae only). Overall, instead  
654 of the red band, the integration of blue and green bands in vegetation indices increases their discriminating power for  
655 SAV (Table 2). These results corroborate the spectral analysis and the CRRS transformations; the blue and green  
656 electromagnetic radiation penetrates deeper through the water allowing more details and information about marine  
657 vegetation discrimination. This finding is consistent with Wicaksono and Hafizt (2013), and Villa et al. (2014) where  
658 the blue band better separates and maps aquatic vegetation features over some lake ecosystems in Italy. However, the  
659 summarized  $R^2$  in Table 2 shows that the indices WAVI, WEVI, and WTDVI provided very close results when  
660 integrating the blue or green bands. Nevertheless, the scatter plots in Fig. 11 (a, b, and c) illustrate that when the green  
661 band is considered instead of the blue, the majority of sampled points are located closer to line 1:1, especially when  
662 the coverage rate becomes denser. This can be explained by the fact that despite the power of blue wavelengths to  
663 penetrate deeper into the water, this band also leads to an overestimation of indices values due to its higher scattering  
664 (Fig. 11), mainly in turbid environments.

## 665 5. Discussion

666 Seagrass and algae species showed similar spectral signature curves, but with subtle differences between species. In  
667 general, some relevant wavelengths are observed for the characterization of the considered species of seagrass and  
668 algae including those at or near 450, 500, 520, 550, 600, 620, 640, 670, and 700 nm. They are related to the absorption  
669 features and reflection peaks due to photosynthetic pigmentations of HU, HS, GA, and BA. Spectral and CRRS  
670 analyses highlighted the importance of the blue, green, and NIR wavelengths for probable differentiation between the  
671 considered seagrass and algae types. However, the magnitude of the  $\Delta\rho$  values among species is an indicator of the  
672 strength of the absorption feature depths and, therefore, of their discriminating power between species. For instance,  
673 the highest  $\Delta\rho$  values among all considered samples (seagrass, algae, and mixed of both) is  $\leq 5\%$  across the visible  
674 wavelengths and around 10 to 15% in NIR. Likewise, the CRRS transformations of all spectra of homogeneous and  
675 mixed samples show that the absorption characteristics become all very similar and, thus, the discrimination between  
676 pure and mixed species becomes difficult or even impossible. These results are in agreement with other findings that  
677 have been conducted in many geographic locations worldwide and have considered many seagrass and algae types.  
678 Considering nine tropical species of seagrass, Wicaksono et al. (2019) showed that even hyperspectral data will not  
679 improve discrimination between seagrass and algae at the species level in pixels or sub-pixels due to the subtle  
680 difference in absorption features among them. As well, Phinn *et al.* (2008) confirmed that the hyperspectral data are  
681 unable to map seagrass biomass at the species level in shallow waters of Moreton Bay in Australia. Using field and  
682 laboratory hyperspectral measurements over several seagrass species on the west coast of Florida, Pu et al. (2012)

683 reported also that the VNIR wavelengths have relatively low accuracies to discriminate among seagrass community  
684 composition.

685 Otherwise, the resampled and convolved spectra in VNIR bands of MSI and OLI sensors are similar in all cases,  
686 considering each species separately or the totality of samples at different coverage rates. These spectra are more  
687 generalized and less precise due to the loss of absorption features caused by pigmentations. Hence, regardless of the  
688 coverage rates, if uniform and homogeneous species are considered, the  $\Delta\rho$  is  $\leq 0.02$  in the visible and is  $\leq 0.22$  in  
689 NIR. While, if all mixed samples and species are considered at the investigated coverage rates,  $\Delta\rho$  is  $\leq 0.05$  in visible  
690 bands and remains stable ( $\Delta\rho \leq 0.22$ ) in NIR. These very small values do not allow spectral distinction among species,  
691 particularly in the visible wavebands. Therefore, based on the multispectral bandwidth of OLI and MSI sensors, it is  
692 difficult to differentiate seagrass and algae individually at the species level. Indeed, it is important to remember that  
693 these simulations were conducted in a Goniometric-Laboratory using close range measurements protocol and  
694 supervising rigorously all measured samples, i.e., homogeneous, or mixed. Moreover, in this controlled environment,  
695 the atmospheric scattering and absorption are absent; errors related to the sensor radiometric calibration are also  
696 absent, no wave's variation, no residual clouds contamination, no sun-glint (specular effects), no variability in water  
697 depth, and no BRDF impact. However, the results obtained are not entirely conclusive and do not provide a clear and  
698 satisfactory distinction among the spectral signatures of the investigated species. The difference among spectral  
699 signatures is surely reduced in the real world when seagrasses and algae are embedded in sediments and overlaid by  
700 water column and constituents including phytoplankton, suspended organic and inorganic matter, variability in water  
701 depth, and remote sensing problems (internal and external). Additionally, the acquired images with Sentinel-MSI (2A  
702 and 2B) and Landsat-OLI (8 and 9) sensors are coded radiometrically in 12 and 16 bits, respectively. These images  
703 cover dissimilar pixels surfaces of 100 m<sup>2</sup> for MSI and 900 m<sup>2</sup> for OLI, where SAV information can be easily mixed  
704 within pixels. Besides, the FOV of these instruments are different, OLI's FOV is 15° covering a swath of 185 km,  
705 while the MSI is characterized by a large FOV of 20.6° covering a swath of 290 km, which requires the adjustments  
706 to reduce differences caused by BRDF effects (acquisition and sun illumination geometries). Data quality may also  
707 change due to the sensor's radiometric performance, SNR, and atmospheric interferences (diffusion and absorption).  
708 Despite corrections of all these anomalies before the information extraction, biases still occur generated by errors  
709 propagation, which affect the recorded signal at the sensor level and, therefore, the precision of discrimination between  
710 seagrass and algae at the species level. For instance, if we consider the published RMSE regarding each source of  
711 error separately, the calculated total RMSE based on errors propagation theory (equation 12) will be approximately  
712 0.08 to 0.10 (reflectance unit). Therefore, this total RMSE is greater than the achieved difference between reflectance  
713 values ( $\Delta\rho \leq 0.05$ ), especially in the visible bands. Accordingly, it is impossible to differentiate between seagrass and  
714 algae at the species level. Likewise, this total RMSE is solely due to the limitations of remote sensing methods, but it  
715 can also be amplified by environmental aspects of seagrass habitat, as discussed above and reported by Wicaksono  
716 and Hafizt (2013).

$$717$$

$$718 \text{RMSE}_{\text{-Total}} = [(\sigma_{\text{-Sensor-drift}})^2 + (\sigma_{\text{-Atmosphere}})^2 + (\sigma_{\text{-Sun-glnt}})^2 + (\sigma_{\text{-BRDF}})^2 + (\sigma_{\text{-Water-column}})^2]^{0.5} \quad (12)$$

719

720 Where:

721  $\sigma_{\text{-Sensor-drift}}$ : Sensor radiometric calibration accuracy,  $\pm 0.03$  (Markham et al., 2014 and 2016),

722  $\sigma_{\text{-Atmosphere}}$ : Atmospheric corrections accuracy, mostly around  $\pm 0.03$  to  $\pm 0.05$  in the visible bands (Vermote et al.,  
723 2016),

724  $\sigma_{\text{-Sun-glnt}}$ : Sun glint correction accuracy,  $\pm 0.05$  (Zorrilla et al., 2019),

725  $\sigma_{\text{-BRDF}}$ : Accuracy of BRDF correction for MSI,  $\pm 0.05$  to  $\pm 0.08$  (Roy et al., 2017),

726  $\sigma_{\text{-Water-column}}$ : Accuracy of water column correction,  $\pm 0.04$  (Zoffoli et al., 2014).

727

728 The results of this research accomplished in the Arabian Gulf species based on spectroradiometric measurements are  
729 consistent with other researches carried out in many geographical regions worldwide. Barillé et al. (2009) showed the  
730 degradation of spectral features when resampled into SPOT-HRV visible bands and, therefore, seagrass species could  
731 no longer be discriminated in these wavelengths. This statement is also in agreement with Wicaksono et al. (2017)  
732 who reported that resampled spectra in MSI and OLI bands do not have sufficient spectral information for seagrass  
733 species discrimination for accurate classification. Using MSI and OLI data with respectively 10 m and 30 m pixel  
734 sizes (i.e., each OLI pixel is represented by 9 MSI pixels), Lyons et al. (2011) reported relatively accurate  
735 discrimination between seagrass meadows spots that are very large with homogenous composition and distinct  
736 boundaries between species. While, the differentiation becomes impossible when the analyzed spots are composed of  
737 diverse species and scattered without clear boundary.

738 Furthermore, to analyze the impact of differences in reflectance exclusively due to dissimilarities in spectral  
739 response function between homologous spectral bands, the scatter-plots between SMI and OLI simulated surface  
740 reflectance values at the top of the atmosphere revealed a very good linear relationship ( $R^2$  of 0.999) between VNIR  
741 homologous bands. The slopes and intercepts are nearly equal to unity and zero, respectively. It is also observed that  
742 independently to the sediments substrate (dark and bright) or the color of used bowls (black or yellow), the  $\Delta\rho$  values  
743 between VNIR homologous bands vary in the range of 0.003 to 0.02, regardless of the observed species (seagrass,  
744 algae and mixed) or the coverage rate. Moreover, the achieved overall RMSD in reflectance values are very small ( $\leq$   
745 0.0015) for all VNIR bands, i.e., smaller than the uncertainty of the radiometric calibration process (0.03) as  
746 demonstrated by Markham et al. (2016). In other respect, all the derived homologous WVI values fit near-perfectly  
747 with the 1:1 line expressing an excellent coefficient of determination ( $R^2$  of 0.99), a slope of 0.99 and intercept equal  
748 to zero. Moreover, the achieved RMSD values between MSI and OLI homologous indices are insignificant ( $\text{RMSD} \leq$   
749 0.01) for all indices regardless of the integrated spectral band (red, green, and blue). These results corroborate the  
750 finding of Wicaksono et al. (2019) who reported that MSI and OLI had similar results for tropical seagrass species  
751 analysis using simulated reflectance spectra and imagery data. Moreover, using simulated data and images acquired  
752 simultaneously with MSI and OLI over a wide variety of land cover types including open shallow water, Mandanici  
753 and Bitelli (2016) showed a very high coefficient of determination ( $R^2$  of 0.98) between homologous bands. Therefore,  
754 these results pointed out that the examined sensors, MSI onboard Sentinel-2A/2B and OLI onboard Landsat-8/9, can  
755 be combined for the marine environment and SAV detection, mapping, and monitoring during shorter time intervals  
756 or for consecutive observations. However, rigorous pre-processing issues (sensors calibration, atmospheric

757 corrections, sun-glint corrections, and BRDF normalization) must be addressed before the joint use of acquired data  
758 with these sensors. Furthermore, we demonstrated that blue and green bands are better than red for seagrass and algae  
759 biomass discrimination, providing the best  $R^2$  and the most insignificant RMSD for the investigated indices. Green  
760 rather than the blue band integration is preferable due to its better sensitivity to pigment content within seagrass and  
761 algae tissues, for its ability to penetrate water, and for its low sensibility to atmosphere and water column scattering.

## 762 6. Conclusions

763 The MSI sensors onboard Sentinel satellites 2A/2B and the OLI instruments installed on Landsat 8/9 satellites are  
764 designed to be similar in the perspective that their data be used together to support global Earth surface reflectances  
765 coverage for science and development applications at medium spatial resolution and near-daily temporal resolution.  
766 However, relative spectral response profiles characterizing the filter's responsivities of these instruments are not  
767 identical between the homologous bands, so some differences are probably expected in the recorded shallow water  
768 reflectance values for seagrass, algae, and mixed species differentiation and mapping. Based on spectral analysis and  
769 CRRS transformation, the results of the present research pointed out subtle spectral differences between seagrass (HU  
770 and HS), algae (green and brown), or mixed species, particularly in the blue, green, and NIR wavelengths. However,  
771 once resampled and convolved in MSI and OLI homologous VNIR bands, similar patterns to the original spectra are  
772 observed but with severe generalisation and loss of specific absorption features. Therefore, mapping seagrass and/or  
773 algae at the species level in shallow marine waters is a very difficult if not impossible task, either using multispectral  
774 bandwidth of MSI and OLI sensors or even hyperspectral data. Moreover, different from these ideal simulations in a  
775 controlled environment, the mapping would be more difficult in a real marine habitat where various species are mixed  
776 and interleaved with each other, as well as the propagation of internal and external errors related to remote sensing  
777 data. Hence, it is recommended to discuss SAV rather than mapping seagrass or algae at the species level.

778 Furthermore, instead of the red band, the integration of the blue and green bands in WVI increases their  
779 discriminating power and ability to map SAV, particularly WAVI, WEVI, and WTDVI indices. These results  
780 corroborate the spectral analysis and the CRRS transformations showing that the blue and green electromagnetic  
781 radiation allows better marine vegetation differentiation. Nevertheless, despite the power of blue wavelength to  
782 penetrate deeper into the water, it also leads to a relative overestimation of dense SAV coverage due to the higher  
783 scattering in this part of the spectrum, particularly in the turbid environment. Furthermore, statistical fits between SMI  
784 and OLI simulated surface reflectance over the considered samples reveal an excellent linear relationship ( $R^2$  of 0.999)  
785 between all homologous VNIR bands. The achieved RMSD values are extremely small between the NIR homologous  
786 bands and insignificant for the other bands ( $\leq 0.0015$ ). Moreover, independently of the analysed samples,  
787 homogeneous (seagrass or algae) or mixed (seagrass plus algae), good agreements ( $0.63 \leq R^2 \leq 0.96$ ) were also  
788 obtained between homologous WVI regardless of the integrated spectral bands (i.e., red, green, and blue), yielding  
789 insignificant RMSD ( $\leq 0.01$ ). These achieved RMSD values for reflectances or WVI's are less than the combined  
790 errors related to sensor radiometric calibration and atmospheric corrections. Accordingly, these results pointed out  
791 that MSI and OLI sensors are spectrally similar and can be combined for high temporal frequency to monitor  
792 accurately the SAV and its distribution in time and space in the shallow marine environment. However, rigorous pre-

793 processing issues such as sensors calibration, atmospheric corrections, BRDF normalisation, sun glint, and water  
794 column corrections must be addressed before the joint use of acquired data with these sensors.

795

796 **7. Data Availability:** All data presented in this paper can be obtained upon request to the corresponding author.

797

798 **8. Author Contributions:** Professor A. Bannari performed the paper conceptualization, field data collection, pre-  
799 processing and processing, results analyses and paper writing. Professor S.T. Ali assisted in the field sampling, the  
800 results analyses and the paper writing. Professor A. Abuhussain assisted in the results interpretation, analyses and  
801 paper writing. All authors have read and agreed to the published version of the manuscript.

802

803 **9. Competing Interests:** The authors declare no conflict of interest.

804

#### 805 **10. Acknowledgements**

806 The authors would like to thank the Arabian Gulf University (Kingdom of Bahrain) for the financial support for the  
807 field data collection, and to Marine and Environment Arabia Consultancy Services (Manama, Bahrain), for providing  
808 photographs and making them available for consultation and public use. Our gratitude goes also to the anonymous  
809 reviewers for their constructive comments.

810

#### 811 **11. References**

812 Anders, K. and Lina, N.: Remote sensing of seagrasses in a patchy multi-species environment. *International Journal*  
813 *of Remote Sensing*, 32(8), 2227 – 2244, 2011.

814 ASD: Analytical Spectral Devices. Technical Guide, 4<sup>th</sup> ed.; ASD Inc.: Boulder, CO, USA. Available online:  
815 <http://www.asdi.com/products-spectroradiometers.asp> (accessed on 30 September 2020), 2015.

816 Bakirman, T. and Gumusay, M. U.: Assessment of Machine Learning Methods for Seagrass Classification in the  
817 Mediterranean. *Baltic J. Modern Computing*, 8(2), 315-326. <https://doi.org/10.22364/bjmc.2020.8.2.07> , 2020.

818 Bannari, A.: Synergy between Sentinel-MSI and Landsat-OLI to Support High Temporal Frequency for Soil Salinity  
819 Monitoring in an Arid Landscape. In: *Research Developments in Saline Agriculture*, edited by Jagdish Chander  
820 Dagar, Rajender Kumar Yadav, and Parbodh Chander Sharma. Published by Springer Nature Singapore Pte Ltd.,  
821 pp. 67-93, ISBN: 978-981-13-5831-9. [https://doi.org/10.1007/978-981-13-5832-6\\_3](https://doi.org/10.1007/978-981-13-5832-6_3), 2019.

822 Bannari, A., Morin, D., Huete, A. R. and Bonn, F.: A Review of Vegetation indices. *Remote Sensing Reviews*, 13,  
823 95-120, 1995.

824 Bannari, A., Asalhi, H. and Teillet, P. M.: Transformed Difference Vegetation Index (TDVI) for Vegetation cover  
825 Mapping. *International Geoscience and Remote Sensing Symposium (IGARSS'2002)*, Toronto, Ontario, 9-13  
826 July, pp. 3053-3055, 2002.

827 Bannari, A., Teillet, P. M., and Landry, R.: Comparaison des réflectances des surfaces naturelles dans les bandes  
828 spectrales homologues des capteurs TM de Landsat-5 et TME+ de Landsat-7. *Revue Télédétection*, 4(3), 263-275,  
829 2004.

- 830 Bannari, A. and Kadhem, G.: MBES-CARIS Data Validation for Bathymetric Mapping of Shallow Water in the  
831 Kingdom of Bahrain on the Arabian Gulf. *Remote Sensing*, 9, 385-404, 2017.
- 832 Bannari, A. and Al-Ali, Z.: Ground Reflectance Factor Retrieval from Landsat (MSS, TM, ETM+, and OLI) Time  
833 Series Data based on Semi-empirical Line Approach and Pseudo-invariant Targets in Arid Landscape.  
834 International Geoscience and Remote Sensing Symposium (IGARSS-2020), July 19-24<sup>th</sup>, Waikoloa, Hawaii,  
835 USA, pp. 5990-5993, 2020.
- 836 Barillé, L., Mouget, J. L., Méléder, V., Rosa, P., Jesus, B.: Spectral response of benthic diatoms with different  
837 sediment backgrounds. *Remote Sensing of Environment*, 115(4), 1034–1042, 2011.
- 838 Barillé, L., Robin, M., Harin, N., Bargain, A. and Launeau, P.: Increase in seagrass distribution at Bourgneuf Bay  
839 (France) detected by spatial remote sensing. *Aquatic Botany*, 92(3), 185-194, 2010.
- 840 Bargain, A., Robin, M., Le-Men, E., Huete, A. R. and Barillé, L.: Spectral response of the seagrass *Zostera noltii* with  
841 different sediment backgrounds. *Aquatic Botany*, 98, 45-56, 2012.
- 842 Bayyana, S., Pawar, S., Gole, S., Dudhat, S., Pande, A., Mitra, D., Johnson, J. A. and Sivakumar, K.: Detection and  
843 mapping of seagrass meadows at Ritchie’s archipelago using Sentinel 2A satellite imagery. *Current Science*,  
844 118(8), 1275-1282. DOI: 10.18520/cs/v118/i8/1275-1282, 2020.
- 845 Ben-Dor, E., Ong, C. and Lau, I. C.: Reflectance measurements of soils in the laboratory: Standards and protocols.  
846 *Geoderma*, 245–246, 112–124, 2015.
- 847 Boström, C., Pittman, S., Kneib, R. and Simenstad, C.: Seascape ecology of coastal biogenic habitats: advances, gaps  
848 and challenges. *Marine Ecology Progress Series*, 427, 191– 217, 2011.
- 849 Burfeind, D. D. and Stunz, G. W.: The effects of boat propeller scarring intensity on nekton abundance in subtropical  
850 seagrass meadows. *Marine Biology (Berlin)*, 148, 953–962, 2006.
- 851 Candra, E. D., Hartono, and Wicaksono, P.: Above Ground Carbon Stock Estimates of Mangrove Forest Using  
852 Worldview-2 Imagery in Teluk Benoa, Bali. *IOP Conference Series: Earth and Environmental Science*, 47(1).  
853 <https://doi.org/10.1088/1755-1315/47/1/012014>, 2016.
- 854 Chen, C.-F., Lau, A.-K., Chang, N.-B., Son, N.-T., Tong, P.-H.-S and Chiang, S.-H.: Multi-temporal change detection  
855 of seagrass beds using integrated Landsat TM/ETM+/OLI imageries in Cam Ranh Bay, Vietnam. *Ecological*  
856 *Informatics*, 35, 43-54, 2016.
- 857 Clark, R. N. and Roush, T. L.: Reflectance spectroscopy: Quantitative analysis techniques for remote sensing  
858 applications. *Journal of Geophysical Research*, 89, 6329–6340, 1984.
- 859 Clark, R. N., King, T. V. V. and Gorelick, N. S.: Automatic continuum analysis of reflectance spectra. In JPL  
860 Proceedings of the 3<sup>rd</sup> Airborne Imaging Spectrometer Data Analysis Workshop, 138-142. Available on line:  
861 <https://ntrs.nasa.gov/archive/nasa/casi.ntrs.nasa.gov/19880004388.pdf> (accessed on 18 March 2021), 1987.
- 862 Clark, R. N., Gallagher, A. J. and Swayze, G. A.: Material absorption-band depth mapping of imaging spectrometer  
863 data using the complete band shape least-squares algorithm simultaneously fit to multiple spectral features from  
864 multiple materials. In: Proceedings of the Third Airborne Visible/Infrared Imaging Spectrometer (AVIRIS)  
865 Workshop, NASA - Jet Propulsion Laboratory Publications, No. 90-54, pp. 176–186, 1990.



- 866 Clark, R. N. and Swayze, G. A.: Mapping minerals, amorphous materials, environmental materials, vegetation, water,  
867 ice and snow, and other materials. The USGS Tricorder algorithm, *in* Green, R.O., ed., Summaries of the fifth  
868 annual NASA Jet Propulsion Laboratory airborne earth science workshop: Pasadena, NASA Jet Propulsion  
869 Laboratory Publication, 95(1), 39-40, 1995.
- 870 Clark, R. N., Swayze, G. A., Carlson, R., Grundy, W. and Noll, K.: Spectroscopy from Space. *Reviews in Mineralogy*  
871 *and Geochemistry*, 78(1), 399-446. DOI:10.2138/rmg.2014.78.10, 2014.
- 872 Crowley, J. K., Brickey, D. W. and Rowan, L. C.: Airborne imaging spectrometer data of the Ruby Mountains,  
873 Montana: mineral discrimination using relative absorption band-depth images. *Remote Sensing of Environment*,  
874 29(2), 121–134. [https://doi.org/10.1016/0034-4257\(89\)90021-7](https://doi.org/10.1016/0034-4257(89)90021-7), 1989.
- 875 Cummings, M. E. and Zimmerman, R. C.: Light harvesting and the package effect in the seagrasses *Thalassia*  
876 *testudinum* Banks ex König and *Zostera marina* L.: Optical constraints on photo-acclimation. *Aquatic Botany*, 75,  
877 261–274, 2003.
- 878 Dahdouh-Guebas, F., Coppejans, E. and Van-Speybroeck, D.: Remote sensing and zonation of seagrasses and algae  
879 along the Kenyan coast. *Hydrobiologia*, 400, 63-73, 1999.
- 880 Dattola, L., Rende, S. F., Dominici, R., Lanera, P., Di-Mento, R., Scalise, S., Cappa, P., Oranges, T. and Aramini, G.:  
881 Comparison of Sentinel-2 and Landsat-8 OLI satellite images vs. high spatial resolution images (MIVIS and  
882 WorldView-2) for mapping *Posidonia oceanica* meadows. Proceedings of SPIE 10784, Remote Sensing of the  
883 Ocean, Sea Ice, Coastal Waters, and Large Water Regions, 10 October 2018, Vol. 10784, 1078419-1; doi:  
884 10.1117/12.2326798, 2018.
- 885 Davranche, A., Lefebvre, G. and Poulin, B.: Wetland monitoring using classification trees and SPOT-5 seasonal time  
886 series. *Remote Sensing of Environment*, 114(3), 552–562, 2010.
- 887 Dean, A. and Salim, A.: Remote sensing for the sustainable development of offshore mariculture. In: *A global*  
888 *assessment of offshore mariculture potential from a spatial perspective*, edited by: Kapetsky, J. M., Aguilar-  
889 Manjarrez, J. and Jenness, J.: FAO Fisheries and Aquaculture Technical Paper N. 549, Rome, Italy, 181 pp, 2013.
- 890 Dekker, A. G., Hestir, E. L., Malthus, T. J. and Thankappan, M.: Continental Scale Aquatic Habitat Monitoring Using  
891 Sentinel-2. ESA-ESRIN, Frascati, Italy, 23 to 27 April; 28 pp, 2012
- 892 Den-Hartog, C.: The seagrasses of the world. North-Holland Publishing Company, Amsterdam, Netherland, 275 pp.  
893 <https://doi.org/10.1002/iroh.19710560139>, 1970.
- 894 Dierssen, H. M., Chlus, A. and Russell, B.: Hyperspectral discrimination of floating mats of seagrass wrack and the  
895 macroalgae *Sargassum* in coastal waters of Greater Florida Bay using airborne remote sensing. *Remote Sensing*  
896 *of Environment*, 167, 247-258, 2015.
- 897 Drusch, M., Del-Bello, U., Carlier, S., Colin, O., Fernandez, V., Gascon, F., Hoersch, B., Isola, C. Laberinti, P.,  
898 Martimort, P., Meygret, A., Spoto, F., Sy, O., Marchese, F., Bargellini, P.: Sentinel-2: ESA's optical high-  
899 resolution mission for GMES operational services. *Remote Sensing of Environment*, 120, 25–36.  
900 <https://doi.org/10.1016/j.rse.2011.11.026>, 2012.

- 901 Duarte, C. M. and Gattuso, J.-P.: Seagrass meadows. In Encyclopedia of Earth. Edited by Cutler J. Cleveland;  
902 Environmental information coalition National Council for Science and the Environment, Washington, DC, USA,  
903 2008.
- 904 Duarte, C. M., Losada, I. J., Hendriks, I. E., Mazarrasa, I. and Marbà, N.: The role of coastal plant communities for  
905 climate change mitigation and adaptation. *Nature Climate Change*, 3(11), 961–968.  
906 <https://doi.org/10.1038/nclimate1970>, 2013.
- 907 Duffy, J. P., Pratt, L., Anderson, K., Land, P. E. and Shutler, J. D.: Spatial assessment of intertidal seagrass meadows  
908 using optical imaging systems and a lightweight drone. *Estuarine, Coastal and Shelf Science*, 200, 169–180, 2018.
- 909 Dunton, K. H., and Schonberg, S. V.: Assessment of propeller scarring in seagrass beds of the south Texas coast:  
910 *Journal Coastal Research*, 37, 100–110, 2002.
- 911 ENVI: Continuum Removal Tutorial. Boulder, Colorado, USA.  
912 <http://www.harrisgeospatial.com/docs/ContinuumRemoval.html> , 2017.
- 913 Erftemeijer, P. L. A. and Shuail, D. A.: Seagrass Habitats in Arabian Gulf: Distribution, Tolerance Thresholds and  
914 Threats. *Aquatic Ecosystem Health and Management*, 15(1), 73-83, 2012.
- 915 Ferguson, R. L. and Wood, L. L.: Mapping Submerged Aquatic Vegetation in North Carolina with Conventional  
916 Aerial Photography. Federal Coastal Wetland Mapping Programs, National Ocean Pollution Policy Board's  
917 Habitat Loss and Modification Working Group. Biological Report, 90(18), pp. 125 – 132. Also available in web:  
918 <https://apps.dtic.mil/sti/pdfs/ADA322827.pdf#page=123>, 1990.
- 919 Flood, N.: Comparing Sentinel-2A and Landsat 7 and 8 Using Surface Reflectance over Australia. *Remote Sensing*,  
920 9, 659, 2017. DOI: 10.3390/rs9070659, 2017.
- 921 Fourqurean, J. W., Duarte, C. M., Kennedy, H., Marbà, N., Holmer, M., Mateo, M. A., Apostolaki, E. T., Kendrick,  
922 G. A., Krause-Jensen, D., McGlathery, K. D. and Serrano, O.: Seagrass ecosystems as a globally significant carbon  
923 stock. *Nature Geoscience*, 5(7), 505–509, 2012.
- 924 Fyfe, S. K.: Spatial and temporal variation in spectral reflectance: Are seagrass species spectrally distinct? *Limnology*  
925 *and Oceanography*, 48(1, part 2), 464–479. [http://dx.doi.org/10.4319/lo.2003.48.1\\_part\\_2.0464](http://dx.doi.org/10.4319/lo.2003.48.1_part_2.0464), 2003.
- 926 Gascon, F., Bouzinac, C., Thépaut, O., Jung, M., Francesconi, B., Louis, J., Lonjou, V., Lafrance, B., Massera, S.,  
927 Gaudel-Vacaresse, A., Languille, F., Alhammoud, B., Viallefont, F., Pflug, B., Bieniarz, J., Clerc, S., Pessiot, L.,  
928 Trémas, T., Cadau, E., De Bonis, R., Isola, C., Martimort, P. and Fernandez, V.: Copernicus Sentinel-2A  
929 Calibration and Products Validation Status. *Remote Sensing*, 9, 584. <https://doi.org/10.3390/rs9060584>, 2017.
- 930 Gitelson, A. A., Kaufman, Y. J., Stark, R. and Rundquist, D.: Novel algorithms for remote estimation of vegetation  
931 fraction. *Remote Sensing of Environment*, 80, 76–87, 2002a.
- 932 Gitelson, A. A., Stark, R., Grits, U., Rundquist, D., Kaufman, Y. J. and Derry, D.: Vegetation and soil lines in visible  
933 spectral space: a concept and technique for remote estimation of vegetation fraction. *Int. Journal of Remote*  
934 *Sensing*, 23(13), 2537–2562, 2002b.
- 935 Green, E. P. and Short, F.: World atlas of seagrasses. Prepared by the UIMEP World Conservation Monitoring Centre.  
936 University of California Press, Berkeley, USA, Volume 47. Berkeley (California, USA): University of California.  
937 <https://doi.org/10.1515/BOT.2004.029>, 2003.

- 938 Grech, A., Chartrand-Miller, K., Erfemeijer, P., Fonseca, M., McKenzie, L., Rasheed, M. and Coles, R.: A  
939 comparison of threats, vulnerabilities and management approaches in global seagrass bioregions. *Environmental*  
940 *Research Letters*, 7(2), 024006, 2012.
- 941 Hamel, M. A. and Andréfouët, S.: Using very high resolution remote sensing for the management of coral reef  
942 fisheries: review and perspectives. *Marine Pollution Bulletin*, 60(9),1397-405. DOI:  
943 10.1016/j.marpolbul.2010.07.002. Epub 2010 Jul 24, 2010.
- 944 Hashim, M., Misbari, S., Yahya, N. N., Ahmad, S., Reba, M. N. and Komatsu, T.: An approach for quantification of  
945 submerged seagrass biomass in shallow turbid coastal waters. In *Proceedings of IGARSS, Quebec, Canada*, pp.  
946 4439-4442. DOI: 10.1109/IGARSS.2014.6947476, 2014.
- 947 Hedley, J., Roelfsema, C., Koetz, B. and Phinn, S.: Capability of the Sentinel 2 mission for tropical coral reef mapping  
948 and coral bleaching detection. *Remote Sensing of Environment*, 120, 145–155, 2012a.
- 949 Hedley, J. D., Roelfsema, C. M., Phinn, S. R. and Mumby, P. J.: Environmental and sensor limitations in optical  
950 remote sensing of coral reefs: implications for monitoring and sensor design. *Remote Sensing*, 4, 271-302.  
951 <http://dx.doi.org/10.3390/rs4010271>, 2012b.
- 952 Hossain, M. S., Bujang, J. S., Zakaria, M. H. and Hashim, M.: The application of remote sensing to seagrass  
953 ecosystems: An overview and future research prospects. *Int. J. Remote Sensing*, 36(1), 61–113, 2014.
- 954 Huang, Z., Turner, B. J., Dury, S. J., Wallis, I. R. and Foley, W. J.: Estimating foliage nitrogen concentration from  
955 HYMAP data using continuum removal analysis. *Remote Sensing of Environment*, 93, 18–29, 2004.
- 956 Huete, A. R.: A soil-adjusted vegetation index (SAVI). *Remote Sensing of Environment*, 25, 295-309, 1988.
- 957 Huete, A. R., Didan, K., Miura, T., Rodriguez, E. P., Gao, X. and Ferreira, L. G.: Overview of the radiometric and  
958 biophysical performance of the MODIS vegetation indices. *Remote Sensing of Environment*, 83(1), 195-213.  
959 [http://dx.doi.org/10.1016/S0034-4257\(02\)00096-2](http://dx.doi.org/10.1016/S0034-4257(02)00096-2), 2002.
- 960 Hunt, Jr. E. R., Doraiswamy, P. C., McMurtrey, J. E., Daughtry, C. S. T., Perry, E. M., and Akhmedov, B.: A visible  
961 band index for remote sensing leaf chlorophyll content at the canopy scale. *Int. Journal of Applied Earth*  
962 *Observation and Geoinformation*, 21, 103–112, 2013.
- 963 Indayani, A. B., Danoedoro, P., Wicaksono, P., Winarso, G. and Setiawan, K. T.: Spectral Analysis from Absorption  
964 and Reflectance of Seagrass Leaves using Trios-Ramses Spectroradiometer in Nusa Lembongan and Pemuteran,  
965 Bali. *Jurnal Penginderaan Jauh dan Pengolahan Data Citra Digital*, 17(2), 103-113.  
966 <http://dx.doi.org/10.30536/j.pjpdcd.2020.v17.a3384>, 2020.
- 967 Irons, J. R. Dwyer, J. L. and Barsi, J. A.: The next Landsat satellite: the Landsat data continuity mission. *Remote*  
968 *Sensing of Environment*, 122, 11–21. <https://doi.org/10.1016/j.rse.2011.08.026>, 2012.
- 969 Jackson, R. D, Pinter, P. J., Paul, J., Reginato, R. J., Robert, J. and Idso, S. B.: *Hand-Held Radiometry. Agricultural*  
970 *Reviews and Manuals, ARM-W-19; U.S. Department of Agriculture Science and Education Administration:*  
971 *Phoenix, AZ, USA, 1980.*
- 972 James, M. E. and Kalluri, S. N. V.: The Pathfinder AVHRR land data set: an improved coarse resolution data set for  
973 terrestrial monitoring. *Int. Journal of Remote Sensing*, 15(17), 3347–3363, 1994.

- 974 Johnsen, G. and Sakshaug, E.: Biooptical characteristics of PSII and PSI in 33 species (13 pigment groups) of marine  
975 phytoplankton, and the relevance for pulse amplitude-modulated and fast-repetition-rate fluorometry1. *Journal of*  
976 *Phycology*, 43, 1236–1251, 2007.
- 977 Kibele, J.: Submerged habitats from space: Increasing map production capacity with new methods and software. PhD  
978 Thesis, Institute of Marine Science, the University of Auckland, New-Zeeland, 179 pp, 2017.
- 979 Kirk, J. T. O.: *Light and photosynthesis in aquatic ecosystems*, 2<sup>nd</sup> edition. Cambridge university press, 509 pp.  
980 <https://doi.org/10.1017/CBO9780511623370>, 1994.
- 981 Knight, E. and Kvaran, G.: Landsat-8 operational land imager design, characterization and performance. *Remote*  
982 *Sensing*, 6(11), 10286–10305, 2014.
- 983 Knudby, A. and Nordlund, L.: Remote sensing of seagrasses in a patchy multi-species environment. *Int. Journal of*  
984 *Remote Sensing*, 32(8), 2227–2244, 2011.
- 985 Kokaly, R. F., Despain, D. G., Clark, R. N. and Livo, K. E.: Mapping vegetation in Yellowstone National Park using  
986 spectral feature analysis of AVIRIS data. *Remote Sensing of Environment*, 84, 437–456, 2003.
- 987 Komatsu, T., Hashim, M., Nurdin, N., Noiraksar, T., Prathep, A., Stankovic, M., Hoang-Son, T. P., Thu, P. M., Luong,  
988 C. V., Wouthyzen, S., Phauk, S., Muslim, A. M., Yahya, N. N., Terauchi, G., Sagawa, T. and Ken-ichi  
989 Hayashizaki, K.-H.: Practical mapping methods of seagrass beds by satellite remote sensing and ground trothing.  
990 *Coastal Marine Science*, 43(1), 1–25, 2020.
- 991 Konstantinos, T., Spyridon, C. S., Apostolos, P. and Nikolaos, S.: The use of Sentinel-2 imagery for seagrass mapping:  
992 Kalloni Gulf (Lesvos Island, Greece) case study. *Proceedings of the SPIE, Volume 9688, Fourth International*  
993 *Conference on Remote Sensing and Geoinformation of the Environment (RSCy2016)*, 96881F.  
994 [Doi:10.1117/12.2242887](https://doi.org/10.1117/12.2242887), <http://dx.doi.org/10.1117/12.2242887>, 2016.
- 995 Kovacs, E., Roelfsema, C., Lyons, M., Zhao, S. and Phinn, S.: Seagrass habitat mapping: how do Landsat 8 OLI,  
996 Sentinel-2, ZY-3A, and Worldview-3 perform? *Remote Sensing Letters*, 9(7), 686–695, 2018.
- 997 Larkum, A. W. D., Orth, R. J. and Duarte, C. M.: *Seagrasses: Biology, ecology and conservation*. *Seagrasses: Biology,*  
998 *Ecology and Conservation*. <https://doi.org/10.1007/978-1-4020-2983-7>, 2006.
- 999 Leleu, K., Alban, F., Pelletier, D., Charbonnel, E., Letourneur, Y. and Boudouresque, C.F.: Fishers' perceptions as  
1000 indicators of the performance of Marine Protected Areas (MPAs). *Marine Policy*, 36(2), 414-422.  
1001 <https://doi.org/10.1016/j.marpol.2011.06.002>, 2012.
- 1002 Li, J. and Chen, B.: Global Revisit Interval Analysis of Landsat-8 -9 and Sentinel-2A-2B Data for Terrestrial  
1003 Monitoring. *Sensors*, 20, 6631. <https://doi.org/10.3390/s20226631>, 2020.
- 1004 Li, J. and Roy, D. P.: A Global Analysis of Sentinel-2A, Sentinel-2B and Landsat-8 Data Revisit Intervals and  
1005 Implications for Terrestrial Monitoring. *Remote Sensing*, 9, 902. DOI: 10.3390/rs9090902, 2017.
- 1006 Li, S., Ganguly, S., Dungan, J. L., Wang, W. L. and Nemani, R. R.: Sentinel-2 MSI Radiometric Characterization and  
1007 Cross-Calibration with Landsat-8 OLI. *Advances in Remote Sensing*, 6, 147-159. DOI : 10.4236/ars.2017.62011.,  
1008 2017.
- 1009 Li, R., Liu, J.-K., Sukcharoenpong, A., Yuan, J., Zhu, H. and Zhang, S.: A Systematic Approach toward Detection of  
1010 Seagrass Patches from Hyperspectral Imagery, *Marine Geodesy*, 35(3), 271-286, 2012.

- 1011 Li, S.: Seagrass Mapping and Human Impact Evaluation Using Remote Sensing Imagery at Core Banks, North  
1012 Carolina. Duke University, 2018.
- 1013 Lin, C., Gong, Z. and Zhao, W.: The extraction of wetland hydrophytes types based on medium resolution TM data.  
1014 Shengtai Xuebao/Acta Ecologica Sinica, 30(23), 6460–6469, 2010.
- 1015 Loveland, T. R. and Dwyer, J. L.: Landsat: Building a strong future. *Remote Sensing of Environment*, 122, 22–29.  
1016 <https://doi.org/10.1016/j.rse.2011.09.022>, 2012.
- 1017 Lyimo, L. D.: Carbon sequestration processes in tropical seagrass beds. PhD Thesis, Department of Ecology,  
1018 Environment and Plant Sciences, Stockholm University, Sweden, 2016.
- 1019 Lyons M. B., Phinn S. R. and Roelfsema C. M.: Integrating Quickbird Multi-Spectral Satellite and Field Data:  
1020 Mapping Bathymetry, Seagrass Cover, Seagrass Species and Change in Moreton Bay, Australia in 2004 and 2007.  
1021 *Remote Sensing*, 3, 42-64. doi:<http://dx.doi.org/10.3390/rs3010042>., 2011.
- 1022 Lyons, M. B., Phinn, S. R. and Roelfsema, C. M.: Long term land cover and seagrass mapping using Landsat and  
1023 object-based image analysis from 1972 to 2010 in the coastal environment of South East Queensland, Australia.  
1024 *ISPRS Journal of Photogrammetry and Remote Sensing*, 71, 34–46, 2012.
- 1025 Lyons, M. B., Roelfsema, C. M., and Phinn, S. R.: Towards understanding temporal and spatial dynamics of seagrass  
1026 landscapes using time-series remote sensing. *Estuarine, Coastal and Shelf Science*, 20, 42–53, 2013.
- 1027 Mandanici, E. and Bitelli, G.: Preliminary Comparison of Sentinel-2 and Landsat 8 Imagery for a Combined Use.  
1028 *Remote Sensing*, 8, 1014, 2016. DOI:10.3390/rs8121014., 2016.
- 1029 Manevski, K., Manakos, I., Petropoulos, G. P. and Kalaitzidis, C.: Discrimination of common Mediterranean plant  
1030 species using field Spectroradiometry. *Int. J. of Applied Earth Observation and Geoinformation*, 13, 922–933,  
1031 2011.
- 1032 Marcello, J., Eugenio, F., Martín, J. and Marqués, F.: Seabed Mapping in Coastal Shallow Waters Using High  
1033 Resolution Multispectral and Hyperspectral Imagery. *Remote Sensing*, 10, 1208. DOI:10.3390/rs10081208, 2018.
- 1034 Markham, B., Barsi, J., Kvaran, G., Ong, L., Kaita, E., Biggar, S., Czapla-Myers, J., Mishra, N. and Helder, D.:  
1035 Landsat-8 Operational Land Imager Radiometric Calibration and Stability. *Remote Sensing*, 6(12), 12275-12308.  
1036 <https://doi.org/10.3390/rs61212275>, 2014.
- 1037 Markham, B., Jenstrom, D., Masek, J. G., Dabney, P., Pedelty, J. A., Barsi, J.A. and Montanaro, M.: Landsat 9: Status  
1038 and plans. In *Earth Observing Systems XXI; International Society for Optics and Photonics: San Diego, CA, USA;*  
1039 *Volume 9972*, p. 99720G, 2016.
- 1040 Mcfeeters, S. K.: The use of the normalized difference water index (NDWI) in the delineation of open water features.  
1041 *Int. Journal of Remote Sensing*, 17, 1425-1432, 1996.
- 1042 Meehan, A. J., Williams, R. J. and Watford, F. A.: Detecting Trends in Seagrass Abundance Using Aerial Photograph  
1043 Interpretation: Problems Arising with the Evolution of Mapping Methods. *Estuaries*, 28(3), 462-472, 2005.

- 1044 Mount, R. E.: Rapid monitoring of extent and condition of seagrass habitats with aerial photography “mega-quadrats.”  
1045 *Journal of Spatial Science*, 52 (1), 105-119, 2007.
- 1046 Morrison, M. A., Lowe, M. L., Grant, C. M., Smith, P. J., Carbines, G., Reed, J., Bury, S. J. and Brown, J. (2014)  
1047 Seagrass meadows as biodiversity and productivity hotspots. *New Zealand Aquatic Environment and Biodiversity*,  
1048 Report No. 137, 151 pages. <http://www.mpi.govt.nz/news-resources/publications.aspx>, 2014.
- 1049 Mumby, P. J., Green, E. P., Edwards, A. J. and Clark, C. D.: Measurement of Seagrass Standing Crop using Satellite  
1050 and Digital Airborne Remote Sensing. *Marine Ecology Progress Series*, 159, 51-60, 1997.
- 1051 NASA (2014) Landsat-8 Instruments. Available online (accessed on 18 March 2021):  
1052 [http://www.nasa.gov/mission\\_pages/landsat/spacecraft/index.html](http://www.nasa.gov/mission_pages/landsat/spacecraft/index.html), 2014.
- 1053 NASA: Landsat-9 Mission Details. Available online (accessed on 18 March 2021).  
1054 <https://landsat.gsfc.nasa.gov/landsat-9/landsat-9-mission-details/>, 2019.
- 1055 NASA: Landsat-9 overview, continuity the legacy - 2021 and beyond. [https://landsat.gsfc.nasa.gov/landsat-9/landsat-](https://landsat.gsfc.nasa.gov/landsat-9/landsat-9-overview)  
1056 [9-overview](https://landsat.gsfc.nasa.gov/landsat-9/landsat-9-overview), 2021.
- 1057 Naser, H.: Human Impacts on Marine Biodiversity: Macro-benthos in Bahrain, Arabian Gulf. Chapter 7 (pp. 109-126)  
1058 in “The Importance of Biological Interactions in the Study of Biodiversity. Edited by J. LÃ³pez-Pujol, ISBN: 978-  
1059 953-307-751-2. Published by InTech, 390 pp, 2011
- 1060 Neckles, H. A., Kopp, B. S., Peterson, B. J. and Pooler, P. S.: Integrating Scales of Seagrass Monitoring to Meet  
1061 Conservation Needs. *Estuaries and Coasts*, 35(1), 23-46, 2012.
- 1062 Novak, A. B and Short, F. T.: Submerged Aquatic Vegetation: Seagrasses. *Encyclopedia of Natural Resources*, 9  
1063 pages. DOI: 10.1081/E-ENRW-120047540, 2014.
- 1064 Onuf, C. P.: Seagrasses, dredging and light in Laguna Madre, Texas, U.S.A.: *Estuarine, Coastal and Shelf Science*,  
1065 39, 75-91, 1994.
- 1066 Orth, R. J., Carruthers, T. J. B., Dennison, W. C., Duarte, C. M., Fourqurean, J. W., Heck, K. L., Hughes, A. R.,  
1067 Kendrick, G. A., Kenworthy, W. J., Olyarnik, S. Short, F. T., Waycott, M. and Williams, S. L.: A Global Crisis  
1068 for Seagrass Ecosystems. *Bioscience*, 56(12), 987–996. [https://doi.org/10.1641/0006-](https://doi.org/10.1641/0006-3568(2006)56[987:AGCFSE]2.0.CO;2)  
1069 [3568\(2006\)56\[987:AGCFSE\]2.0.CO;2](https://doi.org/10.1641/0006-3568(2006)56[987:AGCFSE]2.0.CO;2), 2006.
- 1070 Pasqualini, V., Pergent-Martini, C., Pergent, G., Agreil, M., Skoufas, G., Sourbes, L. and Tsirika, A.: Use of SPOT 5  
1071 for mapping seagrasses: An application to *Posidonia oceanica*. *Remote Sensing of Environment*, 94(1), 39-45,  
1072 2005.
- 1073 Peneva, E., Griffith, J. A. and Carter, G. A.: Seagrass mapping in the northern Gulf of Mexico using airborne  
1074 hyperspectral imagery: a comparison of classification methods. *Journal of Coastal Research*, 24(4), 850–856, 2008.
- 1075 Perez, D., Islam, K., Hill, V., Zimmerman, R., Schaeffer, B., Shen, Y. and Li, J.: Quantifying Seagrass Distribution  
1076 in Coastal Water with Deep Learning Models. *Remote Sensing*, 12, 1581. DOI:10.3390/rs12101581, 2020.
- 1077 Peterson, B. J. and Fourqurean, J. W.: Large-scale patterns in seagrass (*Thalassia testudinum*) demographics in south  
1078 Florida. *Limnology and Oceanography*, 46(5), 1077-1090, 2001.

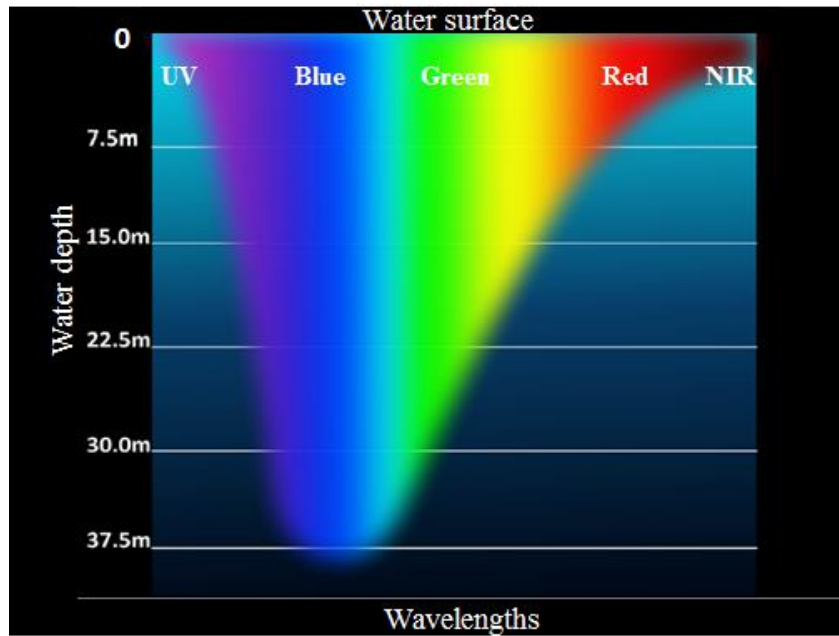
- 1079 Phinn, S., Roelfsema, C., Dekker, A., Brando, V. and Anstee, J.: Mapping seagrass species, cover and biomass in  
1080 shallow waters: An assessment of satellite multispectral and airborne hyper-spectral imaging systems in Moreton  
1081 Bay (Australia). *Remote Sensing of Environment*, 112(8), 3413-3425, 2008.
- 1082 Preen, A.: Distribution, abundance and conservation status of dugongs and dolphins in the southern and western  
1083 Arabian Gulf. *Biological Conservation*, 118(2), 205-218, 2004.
- 1084 Pu, R., Bell, S., Baggett, L., Meyer, C. and Zhao, Y.: Discrimination of Seagrass Species and Cover Classes with *in*  
1085 *situ* Hyperspectral Data. *Journal of Coastal Research*, 28(6),1330-1344, 2012.
- 1086 Richardson, A. J. and Wiegand, C. L.: Distinguishing vegetation from soil background information. *Photogrammetric*  
1087 *Engineering and Remote Sensing*, 43(12), 1541-1552, 1977.
- 1088 Roelfsema, C. M., Lyons, M., Kovacs, E. M., Maxwell, P., Saunders, M. I., Samper-Villarreal, J. and Phinn, S. R.:  
1089 Multi-temporal mapping of seagrass cover, species and biomass: A semi-automated object based image analysis  
1090 approach. *Remote Sensing of Environment*, 150, 172–187, 2014.
- 1091 Roelfsema, C. M., Phinn, S. R., Udy, N. and Maxwell, P.: An integrated field and remote sensing approach for  
1092 mapping seagrass cover, Moreton Bay, Australia. *Journal of Spatial Science*, 54(1), 45–62.  
1093 <https://doi.org/10.1080/14498596.2009.9635166>, 2009.
- 1094 Rouse, J. W., Haas, R. W., Schell, J. A., Deering, D. W., Harlan, J. C. (1974) Monitoring the vernal advancement and  
1095 retrogradation (Greenwave effect) of natural vegetation. NASA/GSFC Type-III Final Report, Greenbelt,  
1096 Maryland, U.S.A., 164 pp, 1974.
- 1097 Roy, D. P., Li, J., Zhang, H. K., Yan, L., Huang, H. and Li, Z.: Examination of Sentinel-2A multi-spectral instrument  
1098 (MSI) reflectance anisotropy and the suitability of a general method to normalize MSI reflectance to nadir BRDF  
1099 adjusted reflectance. *Remote Sensing of Environment*, 199, 25-38. <https://doi.org/10.1016/j.rse.2017.06.019>,  
1100 2017.
- 1101 Roy, D., Zhang, H., Ju, J., Gomez-Dans, J., Lewis, P., Schaaf, C., Sun, Q., Li, J., Huang, H. and Kovalskyy, V.: A  
1102 general method to normalize Landsat reflectance data to nadir BRDF adjusted reflectance. *Remote Sensing of*  
1103 *Environment*, 176, 255–271. <https://doi.org/10.1016/j.rse.2016.01.023>, 2016.
- 1104 Roy, D. P., Wulder, M. A., Loveland, T. R., Woodcock, C. E., Allen, R. G., Anderson, M. C., Helder, D., Irons, J. R.,  
1105 Johnson, D. M., Kennedy, R., Scambos, T. A., Schaaf, C. B., Schott, J. R., Sheng, Y., Vermote, E. F., Belward, A.  
1106 S., Bindschadler, R., Cohen, W. B., Gao, F., Hipple, J. D., Hostert, P., Huntington, J., Justice, C. O., Kilic, A.,  
1107 Kovalskyy, V., Lee, Z. P., Lymburner, L., Masek, J. G., McCorkel, J., Shuai, Y., Trezza, R., Vogelmann, J.,  
1108 Wynne, R. H. and Zhu, Z.: Landsat-8: science and product vision for terrestrial global change research. *Remote*  
1109 *Sensing of Environment*, 145, 154–172. <https://doi.org/10.1016/j.rse.2014.02.001>, 2014.
- 1110 Saarman, E., Gleason, M., Ugoretz, J., Airamé, S., Carr, M., Fox, E., Frimodig, A., Mason, T. and Vasques, J.: The  
1111 role of science in supporting marine protected area network planning and design in California, *Ocean and Coastal*  
1112 *Management*, 74, 45-56. <https://doi.org/10.1016/j.ocecoaman.2012.08.021>, 2013.
- 1113 Sandmeier, St., Muller, Ch., Hosgood, B. and Andreoli, G.: Sensitivity Analysis and quality Assessment of Laboratory  
1114 BRDF Data. *Remote Sensing of Environment*, 64, 176-191, 1998.

- 1115 Short, F. T. and Wyllie-Echeverria, S.: Natural and human-induced disturbance of seagrasses. *Environ. Conserv.*, 23,  
1116 17-27, 1996.
- 1117 Short, F. T. and Coles, R.: *Global Seagrass Research Methods*. Elsevier Publishing, The Netherlands, 482 pp, 2001.
- 1118 Short, F. T., Polidoro, B., Livingstone, S. R., Carpenter, K. E., Bandeira, S., Bujang, J. S., Calumpong, H. P.,  
1119 Carruthers, T. J. B., Coles, R. G., Dennison, W. C., Erfemeijer, P. L. A., Fortes, M. D., Freeman, A. S., Jagtap,  
1120 T. G., Kamal-Abu-Hena, M., Kendrick, G. A., Kenworthy, W. J., La-Nafie, Y. A., Nasution, I. M., Orth, R. J.,  
1121 Prathep, A., Sanciangco, J. C., Tussenbroek, B. V., Vergara, S. G., Waycott, M. W. and Zieman, J. C.: Extinction  
1122 risk assessment of the world's seagrass species. *Biological Conservation*, 144(7), 1961–1971.  
1123 <https://doi.org/10.1016/j.biocon.2011.04.010>, 2011.
- 1124 Silva, T. S. F., Costa, M. P. F., Melack, J. M., and Novo, E. M. L. M.: Remote sensing of aquatic vegetation: Theory  
1125 and applications. *Environmental Monitoring and Assessment*, 140(1-3), 131-145. [https://doi.org/10.1007/s10661-](https://doi.org/10.1007/s10661-007-9855-3)  
1126 [007-9855-3](https://doi.org/10.1007/s10661-007-9855-3), 2008.
- 1127 Skakun, S., Roger, J.-C., Vermote, E. F., Masek, J. G. and Justice, C. O.: Automatic sub-pixel co-registration of  
1128 Landsat-8 Operational Land Imager and Sentinel-2A Multi-Spectral Instrument images using phase correlation  
1129 and machine learning based mapping. *Int. J. of Digital Earth*, 10(12), 1253-1269.  
1130 <http://dx.doi.org/10.1080/17538947.2017.1304586>, 2017.
- 1131 Slater, P. N.: *Remote Sensing - Optics and Optical System*. Addison-Wesley, reading, MA, 575 pp. 1980.
- 1132 Teillet, P. M. and Santer, R.: Terrain Elevation and Sensor Altitude Dependence in a Semi-Analytical Atmospheric  
1133 Code". *Canadian J. of Remote Sensing*, 17, 36-44, 1991.
- 1134 Thakur, Y. et al.: Sea Turtles. Chapter 9, pp. 165–177. In *Marine Environment and Resources of Abu Dhabi*, edited  
1135 by T.Z. Al-Abdessalam, published by Environment Agency of Abu-Dhabi, UAE, 255 pp, 2007.
- 1136 Thorhaug, A., Richardson, A. D. and Berlyn, G. P.: Spectral reflectance of the seagrasses: *Thalassia testudinum*,  
1137 *Halodule wrightii*, *Syringodium filiforme* and five marine algae. *Int. Journal of Remote Sensing*, 28(7), 1487–  
1138 1501, 2007.
- 1139 Traganos, D.: Development of seagrass monitoring techniques using remote sensing data. PhD Thesis, Osnabrück  
1140 University, Osnabrück in Lower Saxony, Germany, 199 pp, 2020.
- 1141 Uhrin, A. V. and Townsend, P. H.: Improved Seagrass Mapping Using Linear Spectral Unmixing of Aerial  
1142 Photographs. *Estuarine, Coastal and Shelf Science*, 171, 11-22, 2016.
- 1143 Umamaheswari, R., Ramachandran, S. and Nobi, E. P.: Mapping the extend of seagrass meadows of Gulf of Mannar  
1144 Biosphere Reserve, India using IRS ID satellite imagery. *Int. Journal of Biodiversity and Conservation*, 1(5), 187-  
1145 193, 2009.
- 1146 Van-Der-Meera, F.: Analysis of spectral absorption features in hyperspectral imagery. *Int. J. Appl. Earth Observation*  
1147 and Geoinformation, 5, 55–68, 2004.
- 1148 Van-der-Werff, H. and Van-der-Meer, F.: Sentinel-2A MSI and Landsat 8 OLI Provide Data Continuity for Geological  
1149 Remote Sensing. *Remote Sensing*, 8, 883. <https://doi.org/10.3390/rs8110883>, 2016.



- 1150 Vermote, E., Justice, C., Claverie, M. and Franch, B.: Preliminary analysis of the performance of the Landsat 8/OLI  
1151 land surface reflectance product. *Remote Sensing of Environment*, 185(2), 46–56.  
1152 DOI: 10.1016/j.rse.2016.04.008, 2016.
- 1153 Villa, P., Bresciani, M., Braga, F. and Bolpagni, R.: Comparative Assessment of Broadband Vegetation Indices over  
1154 Aquatic Vegetation. *IEEE Journal of Selected Topics in Applied Earth Observations and Remote Sensing*, 7(7),  
1155 3117-3127, 2014.
- 1156 Villa, P., Mariano Bresciani, M., Braga, F. and Bolpagni, R.: Mapping Aquatic Vegetation through Remote Sensing  
1157 Data: A Comparison of Vegetation Indices Performances. 6th EARSeL Workshop on Remote S. of the Coastal  
1158 Zone, 7-8 June 2013, Matera, Italy, pp. 10-15, 2013.
- 1159 Wabnitz, C. C., Andréfouët, S., Torres-Pulliza, D., Muller-Karger, F. E. and Kramer, P. A.: Regional-scale seagrass  
1160 habitat mapping in the Wider Caribbean region using Landsat sensors: Applications to conservation and ecology.  
1161 *Remote Sensing of Environment*, 12(8), 3455-3467, 2008.
- 1162 Warren, C., Dupont, J., Abdel-Moati, M., Hobeichi, S., Palandro, D. and Purkis, S.: Remote sensing of Qatar nearshore  
1163 habitats with perspectives for coastal management. *Marine Pollution Bulletin*, 105(2), 641-653.  
1164 <https://doi.org/10.1016/j.marpolbul.2015.11.036>, 2016.
- 1165 Waycott, M., Duarte, C. M., Carruthers, T. J. B., Orth, R. J., Dennison, W. C., Olyarnik, S., Calladine, A.,  
1166 Fourqurean, J. W., Heck Jr., K. L., Hughes, A. R., Kendrick, G. A., Kenworthy, W. J., Short, F. T. and Williams,  
1167 S. L.: Accelerating loss of seagrasses across the globe threatens coastal ecosystems. *PNAS* July 28,  
1168 2009; 106 (30) 12377-12381; [www.pnas.org/cgi/doi/10.1073/pnas.0905620106](http://www.pnas.org/cgi/doi/10.1073/pnas.0905620106), 2009.
- 1169 Wicaksono, P. and Hafizt, M.: Mapping Seagrass from Space: Addressing the Complexity of Seagrass LAI Mapping,  
1170 *European Journal of Remote Sensing*, 46(1), 18-39. <http://dx.doi.org/10.5721/EuJRS20134602>, 2013.
- 1171 Wicaksono, P., Fauzan, M. A., Kumara, I. S. W., Yogyakarta, R. N., Lazuardi, W. and Zhafarina, Z.: Analysis of  
1172 reflectance spectra of tropical seagrass species and their value for mapping using multispectral satellite images.  
1173 *Int. Journal of Remote Sensing*, 40(23), 8955-8977. DOI: 10.1080/01431161.2019.1624866, 2019.
- 1174 Wicaksono, P., Kumara, I. S., Kamal, M., Fauzan, A. M., Zhafarina, Z., Nurswantoro, D. A. and Yogyakarta, R. N.:  
1175 Multispectral Resampling of Seagrass Species Spectra: WorldView-2, Quickbird, Sentinel-2A, ASTER VNIR,  
1176 and Landsat 8 OLI. The 5<sup>th</sup> Geoinformation Science Symposium 2017 (GSS 2017). *IOP Conf. Series: Earth and  
1177 Environmental Science*, 98(2017), 012039. DOI:10.1088/1755-1315/98/1/012039, 2017.
- 1178 Willmott, C.J.: Some comments on the evaluation of model performance. *Bull. Am. Meteorol. Soc.*, 63, 1309-1313,  
1179 1982.
- 1180 Wood, J. S.: Hyperspectral analysis of seagrass in Redfish Bay, Texas. Ph.D. Thesis, Texas A&M University-Corpus  
1181 Christi, Corpus Christi, Texas (USA), 141 pp, 2012.
- 1182 Wulder, M. A., Hilker, T., White, J. C., Coops, N. C., Masek, J. G., Pflugmacher, D. and Crevier, Y.: Virtual  
1183 constellations for global terrestrial monitoring. *Remote Sensing of Environment*, 170, 62–76.  
1184 <https://doi.org/10.1016/j.rse.2015.09.001>, 2015.

- 1185 Yan, L., Roy, D.P., Li, Z., Zhang, H.K. and Huang, H.: Sentinel-2A multi-temporal misregistration characterization  
1186 and an orbit-based sub-pixel registration methodology. *Remote Sensing of Environment*, 215, 495-506.  
1187 <https://doi.org/10.1016/j.rse.2018.04.021>, 2018.
- 1188 Yang, D. and Yang, C.: Seagrass Distribution in China with Satellite Remote Sensing. Chapter 4 in *Remote Sensing*  
1189 *of Planet Earth*, edited by Yann Chemin, pp. 75-94. ISBN: 978-953-307-919-6, InTech. Available from:  
1190 [http://www.intechopen.com/books/remote-sensing-of-planet-earth/seagrass-distribution-in-china-with-](http://www.intechopen.com/books/remote-sensing-of-planet-earth/seagrass-distribution-in-china-with-remotesensing)  
1191 [remotesensing](http://www.intechopen.com/books/remote-sensing-of-planet-earth/seagrass-distribution-in-china-with-remotesensing), 2012.
- 1192 Yang, D. and Yang, C.: Detection of seagrass distribution changes from 1991 to 2006 in Xincun Bay, Hainan, with  
1193 satellite remote sensing. *Sensors*, 9(2), 830-844, 2009.
- 1194 Zhang, H. K. and Roy, D. P.: Computationally inexpensive Landsat-8 operational land imager (OLI) pan-sharpening.  
1195 *Remote Sensing*, 8 (3), 180, 2016.
- 1196 Zhang, H. K., Roy, D. P., Yan, L., Li, Z., Huang, H., Vermote, E., Skakun, S. and Roger, J. C.: Characterization of  
1197 Sentinel-2A and Landsat-8 top of atmosphere, surface, and nadir BRDF adjusted reflectance and NDVI  
1198 differences. *Remote Sensing of Environment*, 215, 482-494. <https://doi.org/10.1016/j.rse.2018.04.031>, 2018.
- 1199 Zhao, D., Lv, M., Jiang, H., Cai, Y., Xu, D. and An, S.: Spatio-Temporal Variability of Aquatic Vegetation in Taihu  
1200 Lake over the Past 30 Years. *PLoS ONE*, 8(6), 6–12. <https://doi.org/10.1371/journal.pone.0066365>, 2013.
- 1201 Zoffoli, M. L., Gernez, P., Rosa, P., Le-Bris, A., Brando, V. E., Barille, A.-L., Harin, N., Peters, S., Poser, K., Spaias,  
1202 L., Peralta, G. and Barille, L.: Sentinel-2 remote sensing of *Zostera noltei*-dominated intertidal seagrass meadows.  
1203 *Remote Sensing of Environment*, 251, 112020, 2020.
- 1204 Zorrilla, N. A., Vantrepotte, V., Ngoc, D.-D., Huybrechts, N. and Gardel, A.: Automated SWIR based empirical sun  
1205 glint correction of Landsat 8-OLI data over coastal turbid water. *Optics Express*, 27(8), A294-A318.  
1206 <https://doi.org/10.1364/OE.27.00A294>, 2019.
- 1207  
1208  
1209  
1210  
1211



1212  
1213 **Figure 1.** Vertical penetration of electromagnetic spectrum in shallow water (adapted from: Morris, 2019),  
1214 [https://commons.wikimedia.org/wiki/Category:Visible\\_spectrum\\_illustrations](https://commons.wikimedia.org/wiki/Category:Visible_spectrum_illustrations))

1215

1216

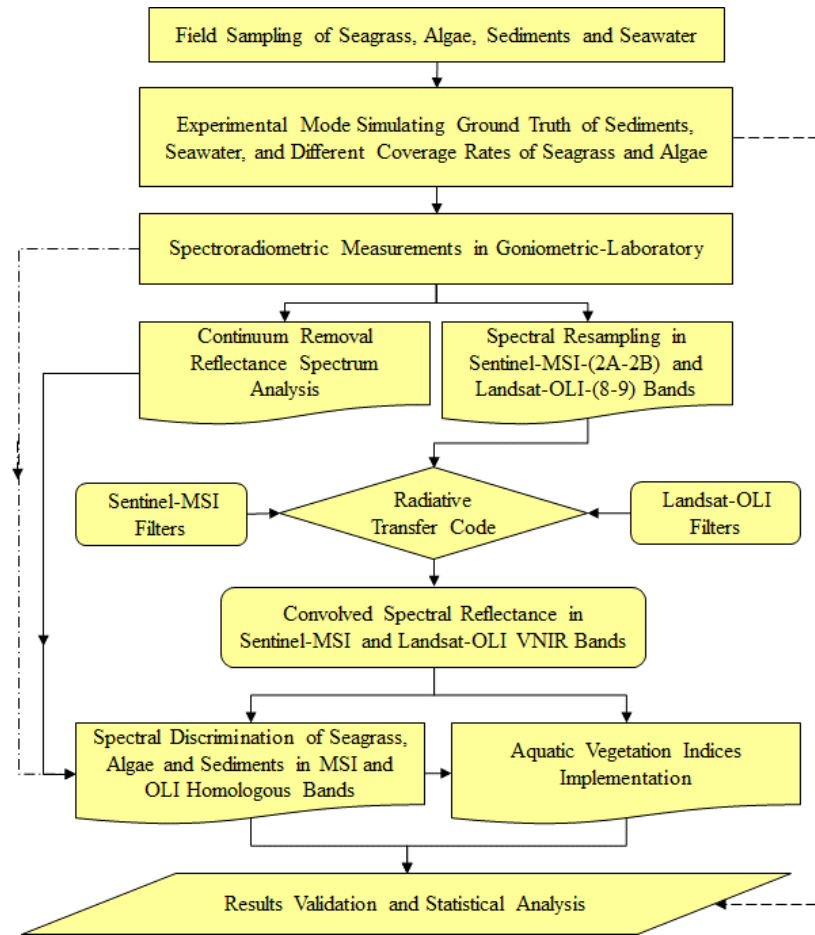
1217

1218

1219

1220

1221



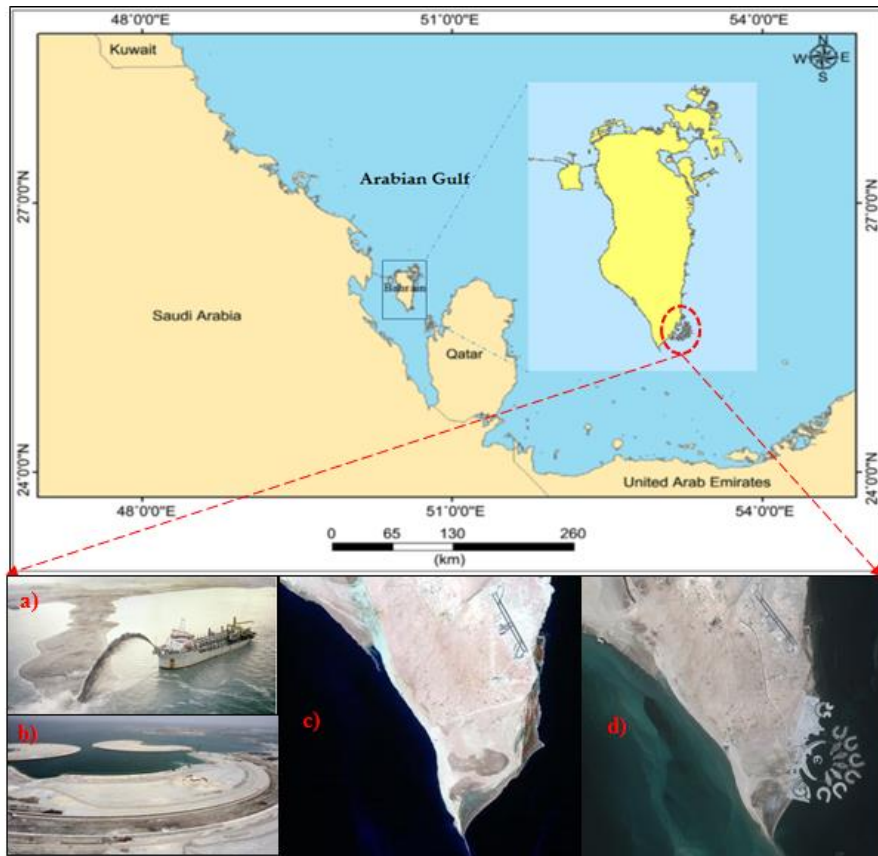
1222

1223 **Figure 2.** Methodology Flowchart

1224

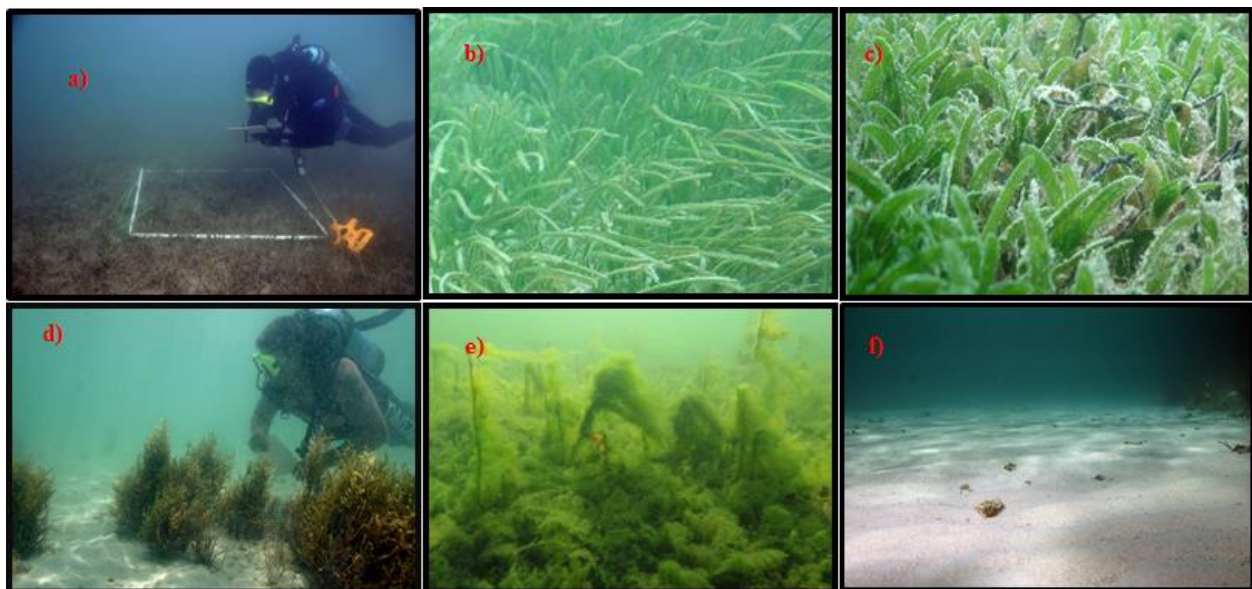
1225

1226



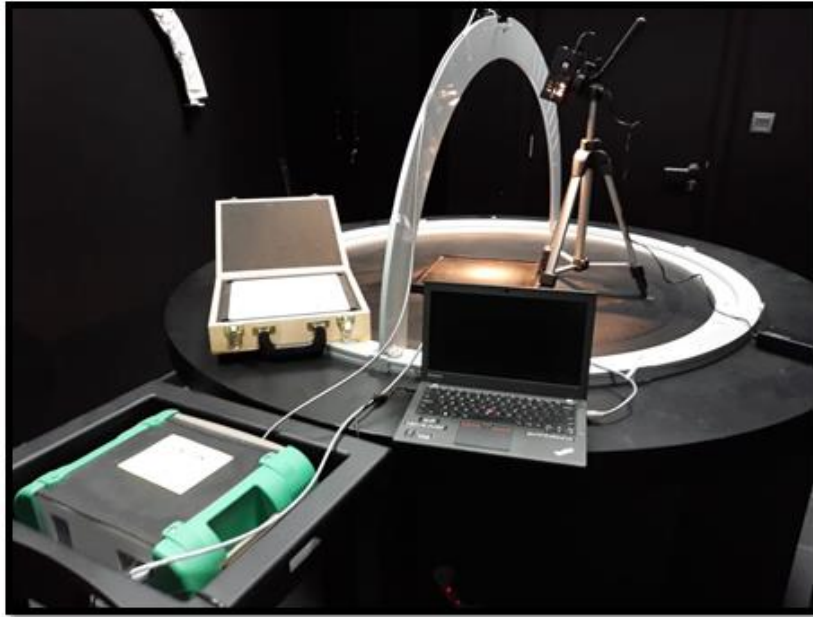
1227  
 1228 **Figure 3.** Study site (Kingdom of Bahrain), photos illustrating dredging operations (a and b), and satellite images of  
 1229 the south part of Bahrain before (c) and after (d) artificial islands construction.

1230



1231  
 1232 **Figure 4.** Diver for sampling operation (a), and underwater photos of the considered seagrass and algae species: HU  
 1233 (b), HS (c), BA (d), GA (e), and bright sediments (f).

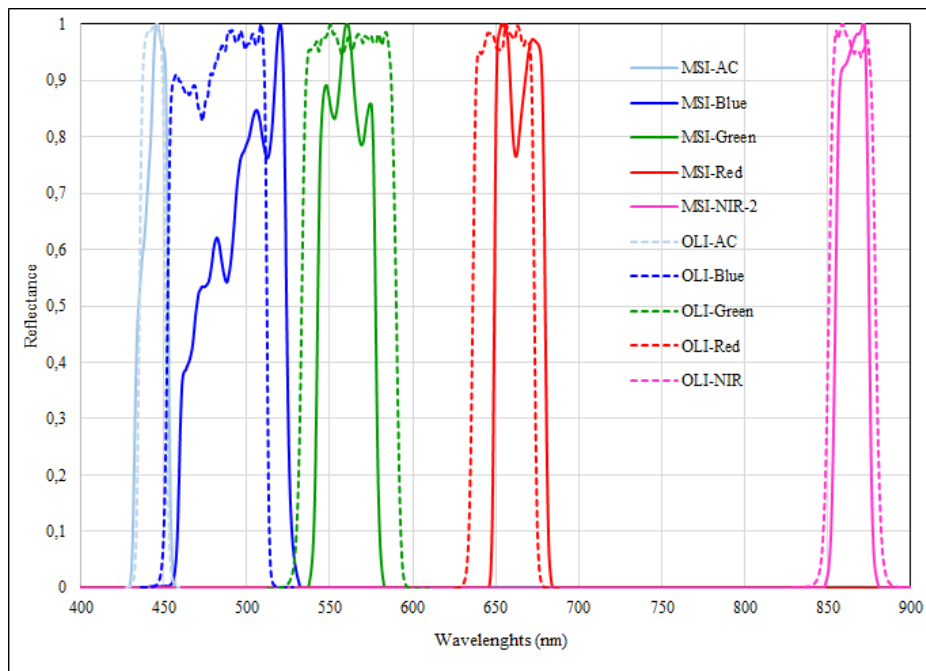
1234



1235

1236 **Figure 5:** Dark Goniometric-Laboratory for ASD measurements.

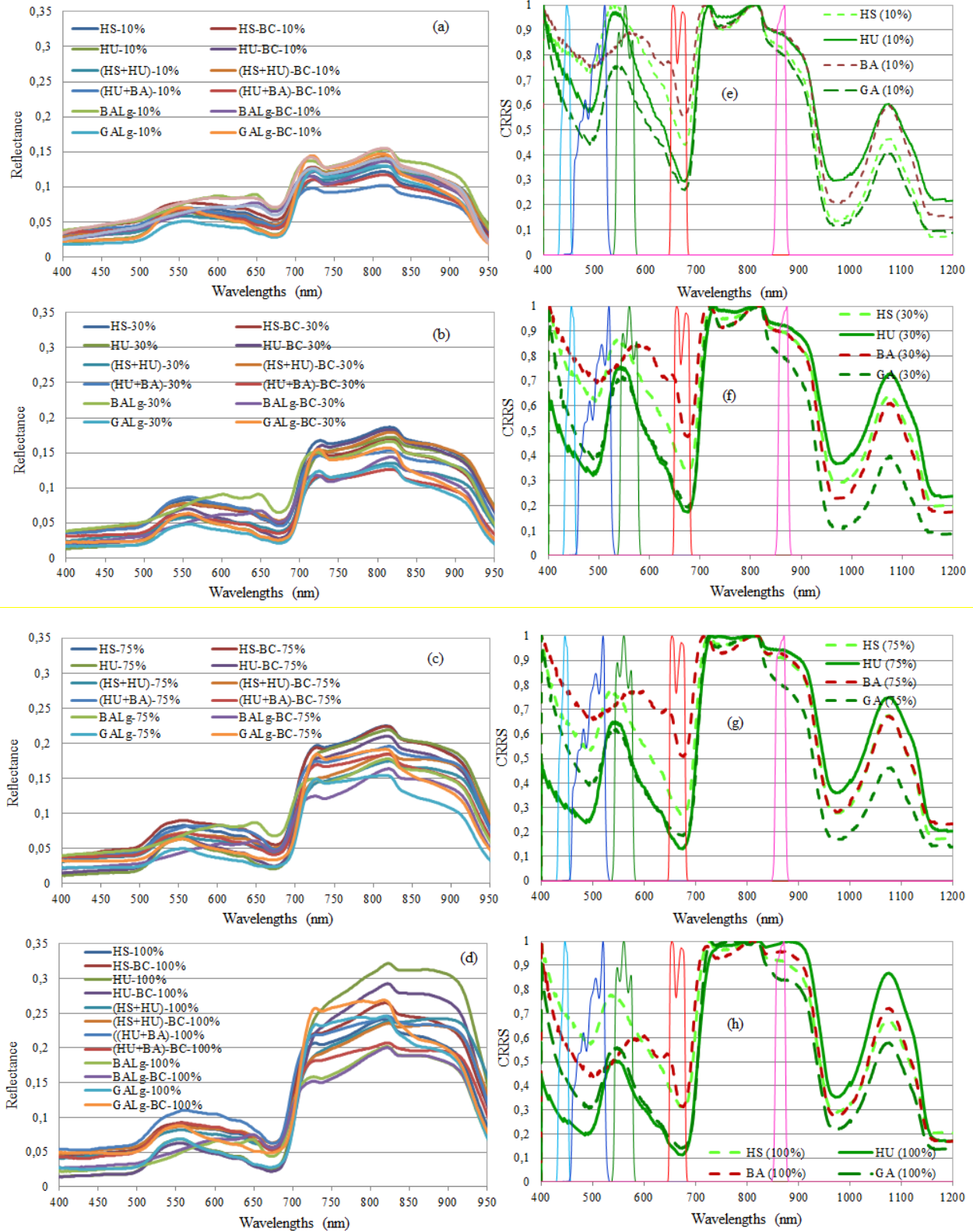
1237



1238

1239 **Figure 6.** Sentinel-MSI and Landsat-OLI relative spectral response profiles characterizing the filters of each spectral  
1240 band in the VNIR.

1241



1242

1243

1244

1245

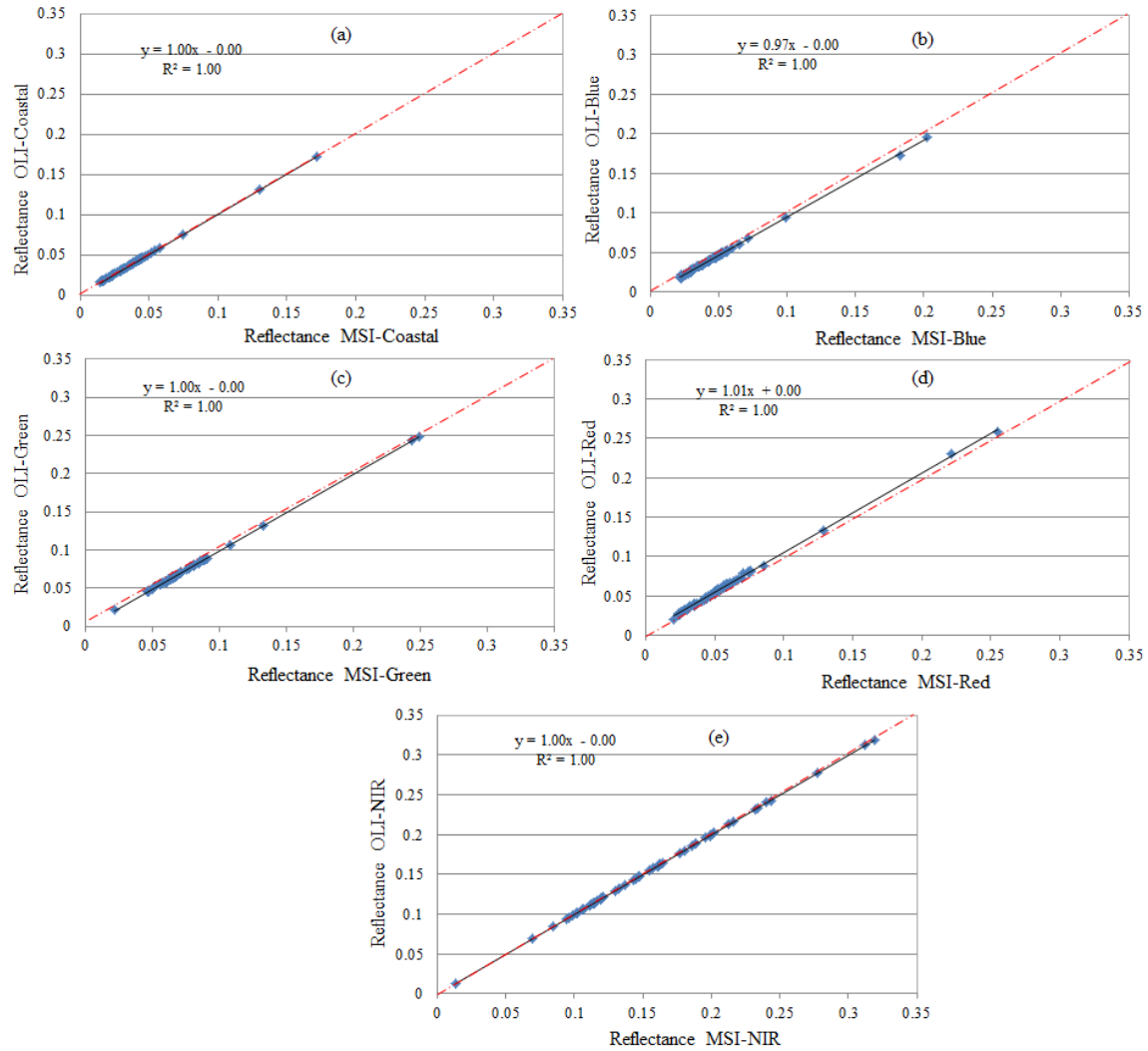
**Figure 7.** Spectral signatures of seagrass and algae samples at different coverage rates (a: 10%, b: 30%, c: 75%, and d: 100%) and their CRRS transformations with the filters of Sentinel-MSI VNIR bands presented in Fig. 6.



1246

1247

1248



1249

1250 **Figure 8.** Scatter-plots of reflectances sampled and convolved in MSI and OLI homologous spectral bands.

1251

1252

1253

1254

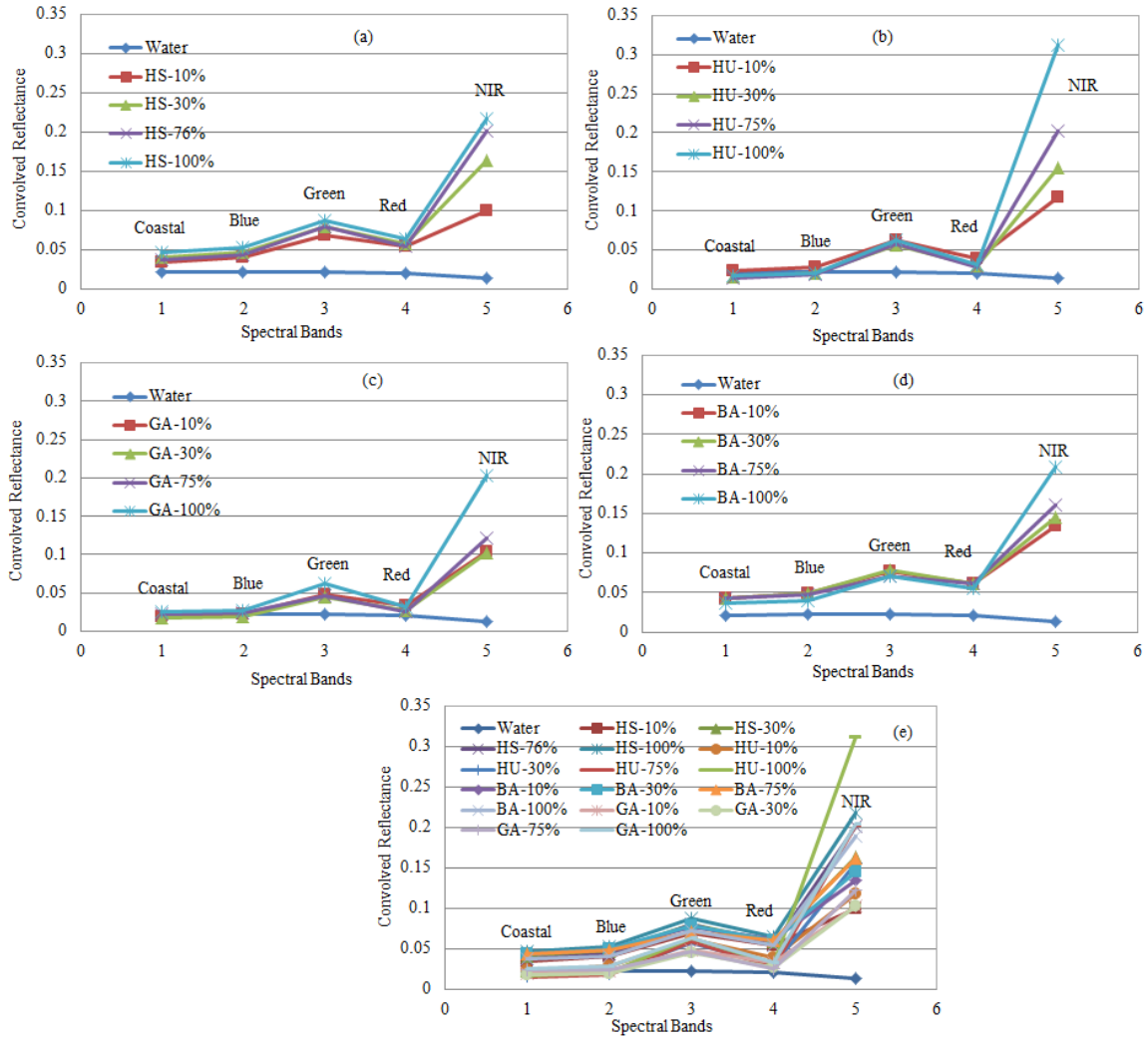
1255

1256

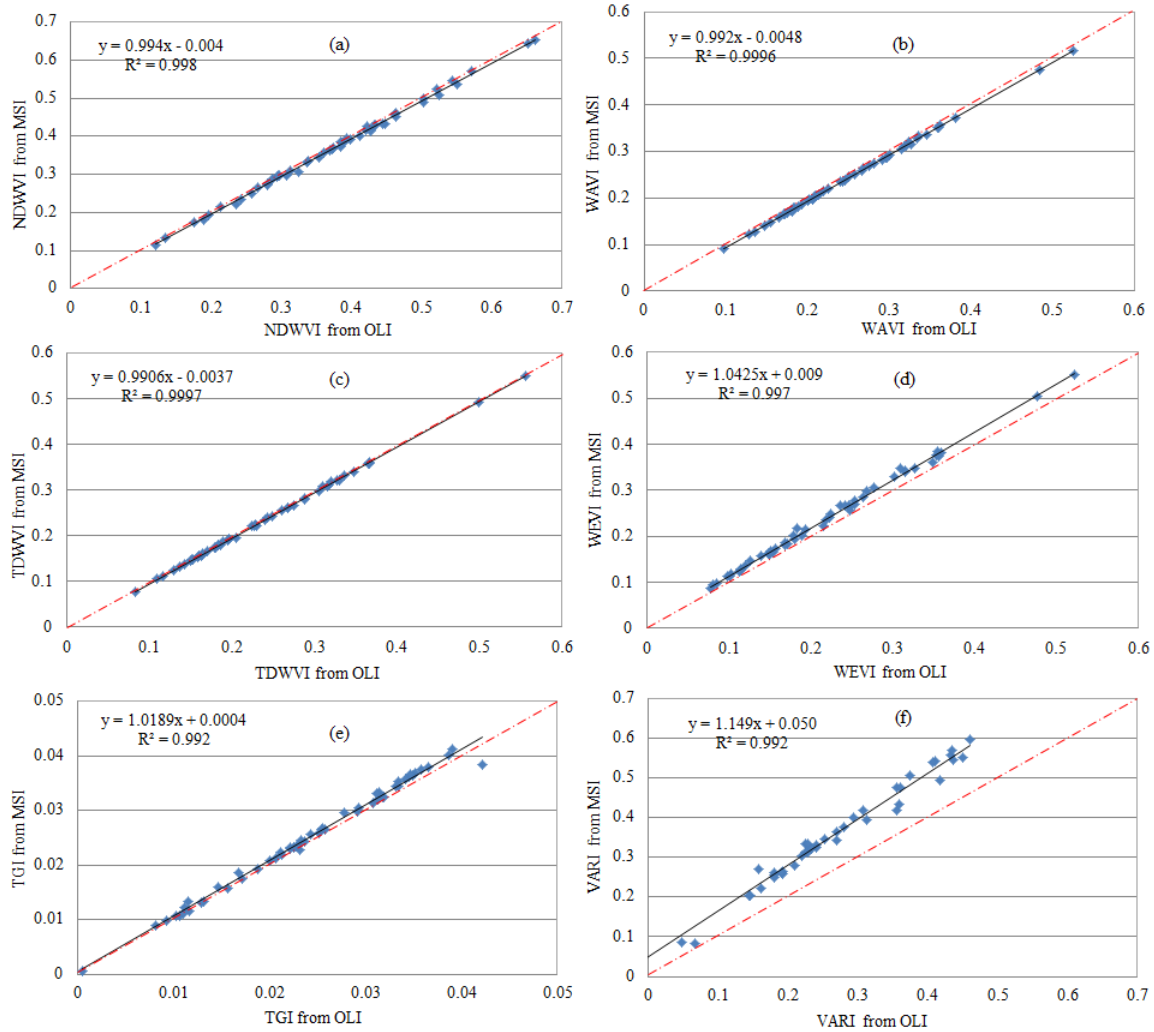
1257



1258  
 1259  
 1260



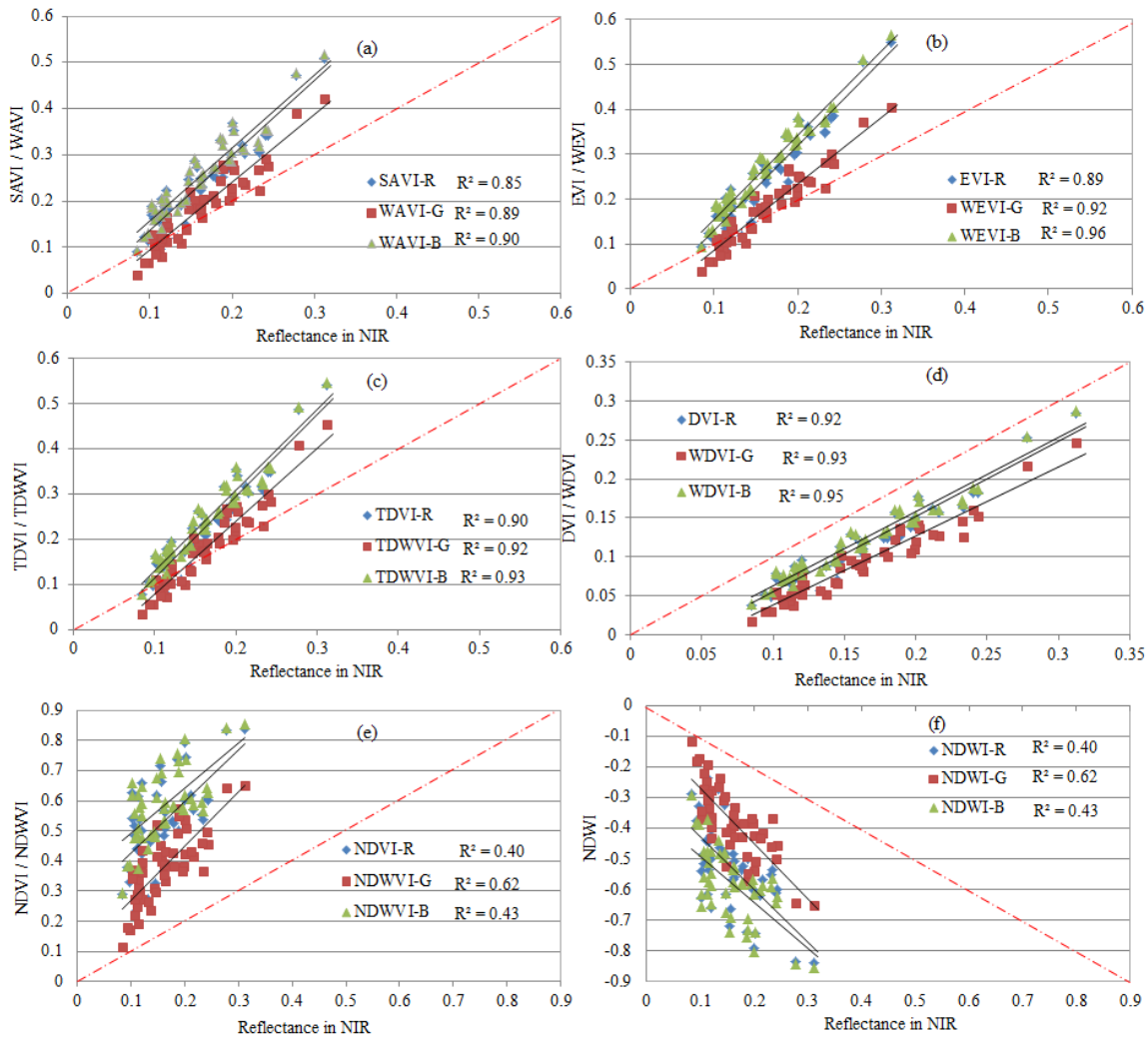
1261  
 1262 **Figure 9.** Seagrass, algae, and seawater reflectances resampled and convolved in VNIR bands of Sentinel-MSI (or  
 1263 Landsat-OLI): HS (a), HU (b), GA (c), BA (d), and all samples (e).  
 1264



1265

1266 **Figure 10.** Scatter-plots of homologous WVI derived from MSI and OLI simulated data.

1267



1268  
 1269 **Figure 11.** Linear regressions ( $p < 0.05$ ) between WVI and reflectance in NIR considering all samples, and integrating  
 1270 the red, green, and blue bands.  
 1271

1272 **Table 1.** The Sentinel-MSI and Landsat-OLI effective bandwidths and characteristics ( $\lambda$  = wavelength, SNR = signal  
 1273 to noise ratio,  $L_{ref}(\lambda)$  = reference radiance,  $E_0(\lambda)$  = Extra-atmospheric irradiance, ).

Spectral Bands	Sentinel-MSI					Landsat-OLI				
	$\lambda$ Centre (nm)	$\Delta\lambda$ (nm)	Pixel Size (m)	SNR	$L_{ref}(\lambda)$ ( $w/m^2/Sr/\mu m$ )	$\lambda$ Centre (nm)	$\Delta\lambda$ (nm)	Pixel Size (m)	SNR	$E_0(\lambda)$ ( $w/m^2/\mu m$ )
Coastal	443	20	60	129	129	443	16	30	130	1895.6
Blue	490	65	10	154	128	482	60	30	130	2004.6
Green	560	35	10	168	128	561	57	30	100	1820.7
Red	655	30	10	142	108	655	38	30	90	1549.4
NIR-2	865	20	20	72	52.5	865	28	30	90	951.2
SWIR-1	1609	85	20	100	4	1609	85	30	100	247.6
SWIR-2	2201	187	20	100	1.5	2201	187	30	100	85.5

1274

1275

1276  
 1277 **Table 2.**  $R^2$  ( $p < 0.05$ ) between vegetation indices integrating red, blue, and green bands and the reflectances in NIR  
 1278 for all considered samples, and the RMSD between indices derived from MSI and OLI sensors data.

Index	Used band	$R^2$	RMSD* in %	Index	Used band	$R^2$	RMSD* in %	Index	Used band	$R^2$	RMSD* in %
NDVI	R	0.40	1.0	TDVI	<b>R</b>	<b>0.90</b>	0.3	DVI	<b>R</b>	<b>0.92</b>	0.2
	<b>G</b>	<b>0.63</b>	0.5		<b>G</b>	<b>0.92</b>	0.2		<b>G</b>	<b>0.93</b>	0.1
	B	0.43	1.0		<b>B</b>	<b>0.93</b>	0.2		<b>B</b>	<b>0.95</b>	0.1
SAVI	R	0.85	0.3	EVI	R	0.89	0.9	NDWI	R	0.40	1.0
	<b>G</b>	<b>0.89</b>	0.2		<b>G</b>	<b>0.92</b>	0.3		<b>G</b>	<b>0.63</b>	0.5
	<b>B</b>	<b>0.90</b>	0.2		<b>B</b>	<b>0.96</b>	0.3		B	0.43	1.0
TGI		0.20	0.1	Diff(G-B)		0.63	0.1	VARI		0.63	3.0

1279 \* is the RMSD between indices derived from MSI and OLI simulated data. The bold type highlight the significant  $R^2$ .

1280

1281